Report No. CDOT-DTD-R-2003-13
Final Report

STUDIES ON THE USE OF HIGH-PERFORMANCE CONCRETE AND FRP REINFORCEMENT FOR THE I-225/PARKER ROAD BRIDGE

P. Benson Shing
Yunping Xi

December 2003

COLORADO DEPARTMENT OF TRANSPORTATION
RESEARCH BRANCH

1. Report No. CDOT-DTD-R-2003-13	2. Government Accession No.	3. Recipient's Catalog No.	
4. Title and Subtitle STUDIES ON THE USE OF HIGH- PERFORMANCE CONCRETE AND FRP REINFORCEMENT FOR THE I-225/PARKER ROAD BRIDGE		5. Report Date December 2003	
		6. Performing Organization Code	
7. Author(s) P. Benson Shing and Yunping Xi		8. Performing Organization Report No. CDOT-DTD-R-2003-13	
9. Performing Organization Name and Address University of Colorado Department of Civil, Environmental & Architectural Engineering Boulder, CO 80309-0428		10. Work Unit No. (TRAIS)	
		11. Contract or Grant No. 00HAA 00069	
12. Sponsoring Agency Name and Address Colorado Department of Transportation - Research 4201 E. Arkansas Ave. Denver, CO 80222		13. Type of Report and Period Covered Final Report	
		14. Sponsoring Agency Code File: 81.30	

15. Supplementary Notes
Prepared in cooperation with the US Department of Transportation, Federal Highway Administration

16. Abstract
The Colorado Department of Transportation (CDOT) recently completed a bridge structure at the I-225/Parker Road Interchange southeast of Denver using innovative construction materials. Part of the bridge deck was constructed of a crack resistant high-performance concrete (HPC) mix and fiber reinforced polymeric reinforcement (FRP) under the sponsorship of the Innovative Bridge Research and Construction (IBRC) program of the Federal Highway Administration (FHWA). To support and validate the design of the bridge deck using innovative materials, a series of studies were conducted at the University of Colorado at Boulder. The studies include the development of HPC mixes, evaluation of the mechanical properties of FRP reinforcing bars under static and cyclic fatigue loads with environmental preconditioning, evaluation of the load carrying capacities of full-scale precast panels prestressed with FRP tendons, and finally, evaluation of the long-term fatigue endurance of a model bridge deck, part of which had a design similar to the actual bridge deck with FRP reinforcement at I-225/Parker Road. Furthermore, the applicability of the AASHTO empirical method to the topping slab of precast panel decks was also investigated. A rational limit-state design method that can result in a significant reduction of deck reinforcement as compared to the conventional design method of AASHTO has been developed as an alternative to the empirical method. This report summarizes the test procedures and outcomes of these studies. Detailed information on these studies can be found in the original reports contained in the attached CD.

Implementation:

The HPC and FRP reinforcement studied in this project were already used by CDOT in the I-225/Parker Road project. This project provided an excellent opportunity for both CDOT and the contractors to become familiar with the handling, performance, and overall use of HPC and FRP products in bridge construction. Results of the reported studies validate the applicability of FRP products for bridge construction and provide useful guidance on the use of such materials for future projects. The HPC developed in this project is now widely used by CDOT for bridge deck construction.

17. Keywords high-performance concrete, shrinkage cracks, fiber-reinforced polymeric reinforcement, precast panel bridge decks, prestress, fatigue endurance		18. Distribution Statement No restrictions. This document is available to the public through: National Technical Information Service 5825 Port Royal Road Springfield, VA 22161	
19. Security Classif. (of this report) None	20. Security Classif. (of this page) None	21. No. of Pages 76	22. Price

Form DOT F 1700.7 (8-72)   Reproduction of completed page authorized

STUDIES ON THE USE OF HIGH-PERFORMANCE CONCRETE AND FRP REINFORCEMENT FOR THE I-225/PARKER ROAD BRIDGE

by

P. Benson Shing
Yunping Xi

Department of Civil, Environmental
& Architectural Engineering
University of Colorado
Boulder, CO 80309-0428

ACKNOWLEDGEMENTS

EXECUTIVE SUMMARY

The Colorado Department of Transportation (CDOT) recently completed a bridge structure at the I-225/Parker Road Interchange southeast of Denver using innovative construction materials. The bridge consists of post-tensioned cast-in-place reinforced concrete box girders with precast prestressed panels as stay-in-place forms and a cast-in-place topping slab for the deck. Part of the bridge deck was constructed of a crack resistant high-performance concrete (HPC) mix and fiber reinforced polymeric reinforcement (FRP) under the sponsorship of the Innovative Bridge Research and Construction (IBRC) program of the Federal Highway Administration (FHWA). The remaining portion was constructed with regular concrete and steel reinforcement. The goal of this was to explore the use of innovative materials to prolong the life span of a bridge by reducing corrosion problems.

To support and validate the design of the bridge deck using innovative materials, a series of studies were conducted at the University of Colorado at Boulder. The studies include the development of HPC mixes, evaluation of the mechanical properties of FRP reinforcing bars under static and cyclic fatigue loads with environmental preconditioning, evaluation of the load carrying capacities of full-scale precast panels prestressed with FRP tendons, and finally, evaluation of the long-term fatigue endurance of a model bridge deck, part of which had a design similar to the actual bridge deck with FRP reinforcement at I-225/Parker Road. Furthermore, the applicability of the AASHTO empirical method to the topping slab of precast panel decks was also investigated. A rational limit-state design method that can result in a significant reduction of deck reinforcement as compared to the conventional design method of AASHTO has been developed as an alternative to the empirical method. This report summarizes the test procedures and outcomes of these studies. Detailed information on these studies can be found in the original reports contained in the attached CD.

The HPC developed in this study has a low early strength and low heat of hydration, and is, therefore, more resistant to temperature and shrinkage cracks. It also has low chloride permeability. The HPC can thus significantly deter the deterioration of bridge decks caused by chloride penetration and the subsequent corrosion of the reinforcing steel. Two mix designs are

recommended for use in the summer and in the winter, respectively. For these mixes, the desired range of cement content is from 465 to 485 lb/yd^3, water/cementitious material ratio from 0.37 to 0.41, and Class F fly ash from 20% to 25%. Class F fly ash is found to result in better durability performance than Class C fly ash.

In order for FRP reinforcing bars to be successfully implemented in roadway construction projects, it is essential to develop a firm understanding of the durability properties of FRP bars and the effects of exposure to severe and frequently changing environments. To this end, the mechanical properties of carbon and glass fiber reinforced polymeric (CFRP and GFRP) reinforcing bars after freeze-thaw exposure were studied. Each specimen requiring pre-conditioning was subjected to low temperature thermal cycling between 68°F (20°C) and –20°F (-29°C) temperature excursions with a 1-hour hold at –20°F and 20-minute hold at 68°F, achieving an 8 cycle per day rate. Specimens were exposed to 250 freeze-thaw cycles corresponding to 750 hours of exposure. Furthermore, the effect of the rate of loading on the tensile strength properties of GFRP bars was investigated to establish a basis for cyclic fatigue loading procedures. There were noticeable increases in strength and marked changes in fracture appearance with increased loading rate. Results of this study show that freeze-thaw exposure may have some effects on the fatigue properties of FRP bars. The degree of deterioration of the FRP bars depends on the temperature ranges and number of freeze-thaw cycles applied. Under the temperature conditions applied in this study, the decrease of the tensile strength of the FRP bars was no more than 10%.

The bonding characteristics of FRP bars were investigated by pullout tests. The test results show that 13-mm (0.5-in) C-BAR (GFRP) reinforcing rods provided higher bond strength than #4 (13-mm diameter) black steel reinforcing bars. The average bond strength of the C-BAR with an embedment of $5d_b$ was 3.15 ksi. The average bond strength of the reinforcing steel with an embedment of $6d_b$ was 2.9 ksi. Furthermore, pullout test results show that 10-mm (0.39-in) Leadline (CFRP) prestressing tendons provided higher bond strength than 3/8-in steel prestressing strand. The average bond strength of the Leadline with an embedment of $10d_b$ was 1.58 ksi. The average bond strength of the steel strand with an embedment of $20d_b$ was 0.99 ksi.

To validate the performance of the precast panels used in the I-225 bridge, full-size panels prestressed with Leadline CFRP rods and steel tendons were tested. Two of the panels had topping slabs and two without. Unfortunately, the panels prestressed with CFRP could not be directly compared to those prestressed with steel due to some abnormalities and defects in the CFRP prestressed panels. However, a careful analysis has indicated that the CFRP prestressed panels should have performed satisfactorily if they were constructed properly. To have a better confirmation of the load carrying capacity, an additional CFRP prestressed panel that was constructed without defects was tested. This panel was removed from the actual bridge. It was found that its load carrying capacity was larger than the theoretical load carrying capacity used in the design.

Finally, to assess the long-term performance of a bridge deck that had CFRP prestressed panels and to evaluate the performance of deck segments designed with the AASHTO conventional method, AASHTO empirical method, and the proposed limit-state design method, a fatigue test was conducted on a model deck. The test results have shown that the portion of the bridge deck that had CFRP prestressed panels demonstrated the same performance as that with steel prestressed panels. Furthermore, the segments of the deck that had the topping slab designed with the empirical method and the limit-state method exhibited the same performance as that designed with the conventional method, even though the latter required 70% more reinforcement in the topping slab. Furthermore, with the use of the empirical method, the segment of the deck that had precast panels performed better than the full-depth cast-in-place segment due to the enhanced strength and crack resistance introduced by the prestressed panels.

The use of the AASHTO empirical method for the design of the topping slab of a precast panel deck does not seem to jeopardize the deck performance under fatigue load cycles. The empirical method can lead to a significant reduction of the top reinforcement in such a deck. It will not only save construction costs, but will also prolong the life span of a bridge deck that has steel reinforcement by reducing corrosion problems. Therefore, it is recommended that the empirical method be allowed for the design of the topping slab in precast panel decks.

TABLE OF CONTENTS

1. Introduction

The Colorado Department of Transportation (CDOT) recently completed a bridge structure at the I-225/Parker Road Interchange southeast of Denver using innovative construction materials. As shown in Figures 1.1 and 1.2, the bridge consists of post-tensioned cast-in-place reinforced concrete box girders with precast prestressed panels as stay-in-place forms and a cast-in-place topping slab for the deck. Part of the bridge deck was constructed of a crack resistant high-performance concrete (HPC) mix and fiber reinforced polymeric reinforcement (FRP) under the sponsorship of the Innovative Bridge Research and Construction (IBRC) program of the Federal Highway Administration (FHWA). The goal of this was to explore the use of innovative materials to prolong the life span of a bridge by reducing corrosion problems.

In recent years, the cracking of reinforced concrete bridge decks has been a major concern in Colorado as well as in many other states. This has been mainly attributed to the use of high early strength concrete that has a high modulus of elasticity and low creep at early age. These properties, combined with the large amount of heat generated during the hydration process, which is typical of high-strength concrete, can lead to excessive shrinkage and temperature cracks in bridge decks. To address this problem, HPC mix designs that have high fly-ash content were developed at the University of Colorado at Boulder (CU) and applied to the reinforced concrete deck in the I-225 bridge. The HPC has a low early strength and low heat of hydration, and is, therefore, more resistant to temperature and shrinkage cracks. It also has low chloride permeability. The HPC can thus significantly deter the deterioration of bridge decks generally caused by chloride penetration and the subsequent corrosion of the reinforcing steel.

The use of FRP for prestressing and reinforcing concrete structures has received increasing attention in the last decade. The benefits of using FRP tendons and bars are that they are non-corrosive, lightweight, non-conductive, magnetically neutral, and extremely strong in tension. The corrosion resistance of FRP reinforcement is highly beneficial to bridges, whose service life is often limited by the corrosion of the reinforcement.

Figure 1.1 – I-225/Parker Road Bridge under Construction

In the I-225 bridge project, some of the precast deck panels were prestressed with carbon fiber reinforced polymeric (CFRP) tendons and the rest with regular seven-wire steel strands. It was the first time CFRP bars were used in such fashion. Furthermore, deformed glass fiber reinforced polymeric (GFRP) bars were used as temperature reinforcement for the panels prestressed with CFRP bars, and also as the main reinforcement for some of the bridge rails. As shown in Figure 1.2, the precast panels were supported on two cast-in-place, post-tensioned concrete box girders. A topping slab was added to the panels to form a composite bridge deck to carry the traffic load. One main problem with FRP reinforcement is that it has to be handled with care. It could be easily damaged at a construction site. Hence, to avoid the complication of using FRP bars at the construction site, where quality control was often more difficult, the

topping slab was reinforced with regular epoxy-coated bars.

Figure 1.2 – Precast Panels Supported on Two Box Girders

Because of the lack of standard design provisions for FRP reinforced concrete structures, studies were conducted at the University of Colorado at Boulder to evaluate the mechanical properties of the FRP materials after environmental preconditioning, validate the load carrying capacity of the deck panels, and examine the long-term fatigue endurance of a model bridge deck containing FRP reinforcement. These studies included the tensile tests of FRP bars under static and cyclic fatigue loads after environmental preconditioning, load tests of simply supported deck panels with and without topping slabs, and the evaluation of the long-term performance of such decks by testing a 30-ft. span and 16-ft. wide, 2/3-scale three-girder deck under fatigue loading.

The aforementioned studies are summarized in Chapters 2 through 5 of this report. However, detailed information on the above studies can be found in the following CDOT reports.

1. Xi, Y., Shing, B., and Xie, Z. (2001), "Development of Optimal Concrete Mix Designs for Bridge Decks." Report No. CDOT-DTD-R-2001-11, Colorado Department of Transportation, Denver, CO. (Summarized in Chapter 2 of this report.)

2. Cusson, R. and Xi, Y. (2003), "The Behavior of Fiber-Reinforced Polymer Reinforcement in Low Temperature Environmental Climates." Report No. CDOT-DTD-R-2003-04, Colorado Department of Transportation, Denver, CO. (Summarized in Chapter 3 of this report.)

3. Zylstra, R., Shing, P.B., and Xi, Y. (2001), "Evaluation of FRP Prestressed Panels/Slabs for I-225/Parker Road Project." Report No. CDOT-DTD-R-2001-14, Colorado Department of Transportation, Denver, CO. (Summarized in Chapter 4 of this report.)

4. Shing, P.B., Borlin, K.A., and Marzahn, G. (2003), "Evaluation of a Bridge Deck with CFRP Prestressed Panels under Fatigue Load Cycles." Report No. CDOT-DTD-R-2003-11, Colorado Department of Transportation, Denver, CO. (Summarized in Chapter 5 of this report.)

These reports can be found in the CD that accompanies this summary report. The fourth report by Shing, Borlin, and Marzahn (2003) also presents a rational limit-state design method for bridge decks. The main distinction of this method as compared to conventional deck design methods is that it accounts for the girder deflections and arching mechanism in bridge decks. By taking into account the lower negative bending moment in a deck induced by girder deflections and the increased moment resistance developed from the arching action, the quantity of reinforcement in a deck slab can be significantly reduced. Many advantages are associated with reduced reinforcement. First, the construction costs will be lowered, including both the material and labor costs. This is especially attractive for FRP reinforced bridge decks. For the case of steel reinforced bridge decks, the service life will be extended and typical maintenance problems associated with concrete spalling and reinforcement corrosion will be minimized.

2. Development of Optimal Concrete Mix Designs for Bridge Decks

2.1 Introduction

Field inspections and a recent study report (Shing and Abu-Hejleh 1999) showed that the cracking problem of bridge decks in Colorado has not been completely resolved, and therefore, there is a pressing need for further improvement of the concrete mix designs currently used in Colorado for concrete bridge decks.

To address the aforementioned issue, a study that consisted of two phases was carried out in this project as reported in detail by Xi et al. (2001). Based on an extensive literature review, the recommended concrete mix in the report by Shing and Abu-Hejleh (1999), and input from the concrete specialists of CDOT, 18 mix designs were formulated in the Phase I study in order to single out some good mix designs satisfying the selected strength, and the chloride permeability and durability requirements. The Phase II study was mainly a fine-tuning of the mixes selected from Phase I and finalization of the mix designs to be used in the field. The recommended concrete mixes are characterized by good workability, proper air content, adequate strength, low chloride permeability, and low drying shrinkage potential.

2.2 Test Methods

The following tests were conducted to evaluate the properties of the concrete.

- Compressive strength tests. The strength tests were performed at 3 days, 7 days, 28 days, and 56 days. For these tests, 4" by 8" cylinders were used. Two cylinders were used for each test at 3 days, 7 days, 28 days, and 56 days.

- Rapid chloride permeability tests (ASTM C 1202, AASHTO T277 "Electrical Indication of Concrete's Ability to Resist Chloride Ion Penetration"). The permeability tests were performed at 28 days and 56 days. Cylindrical specimens of 4" in diameter by 2" in height were used for the permeability tests. Two specimens were used for each test at 28 days and

56 days.

- Crack resistance tests (or ring test, AASHTO PP34-98 " Standard Practice for Estimating the Crack Tendency of Concrete"). Two concrete rings of 6'' in height with outer diameter 18'' and inner diameter 12'' were made for each concrete mix. After one day of curing under room temperature, the molds were removed and the concrete rings were placed in the laboratory (temperature = 72°F and relative humidity = 35%) until the first crack was observed. The cracks were monitored visually by naked eyes as well as by a zoom.

- Drying shrinkage tests (ASTM C-157 " Standard Test Method for Length Change of Hardened Hydraulic-cement Mortar and Concrete"). Two concrete prisms of 3" by 3" by 12" were made for the drying shrinkage tests. After 7 days of curing in a fog room (68°F, 100% Relative Humidity), the prisms were removed from the fog room and placed in the laboratory (temperature 72°F and relative humidity 35%). Shortening of the prisms due to drying shrinkage was then measured. The shrinkage tests were only performed for some concrete mixes.

2.3   Phase I Study

In the Phase I study, cement content (W_c), water-cement ratio (w/c), and fly ash content (W_{fa}) were selected as experimental parameters:

- Three w/c ratios: 0.37, 0.41, 0.45.

- Three W_c values: 450, 485, and 515 lb/yd^3.

- Two W_{fa} values: 20% and 25% of the cement content.

The objective of the Phase I study was to identify the optimal concrete mix design in terms of moderate compressive strength, low chloride permeability, and high crack resistance. A part of

the test results of the Phase I study are listed in Table 2.1.

Table 2.1 – Some of Mix Designs and Test Results of the Phase I Study

		Mix 4-2	Mix 7	Mix 8	Mix 14
Cement content (lb/yd^3)		450	485	485	515
Fly ash lb/yd^3 (% of cement)		112.5 (25)	97 (20)	97 (20)	103 (20)
Silica fume, lb/yd^3 (% of cement)		18 (4)	19.4 (4)	19.4 (4)	20.6 (4)
W/(C+M)		0.37	0.37	0.41	0.41
Sand (lb/yd^3)		1450	1421	1397	1345
Gravel (lb/yd^3)		1595	1595	1595	1595
HRWR (oz/100 lb cement)		10	11.45	12.6	9.72
Micro Air (oz/100 lb cement)		3.36	3.35	3.8	1.17
Retarder (oz/100 lb cement)		3.75	3.8	3.8	2.34
Slump (inch)		1	0	3.5	2
Air content (%)		4.5	7.5	7	5.5
Permeability at 28 days (Coulomb)		3265	2498 2549	2847 3461	2946 2962
Permeability at 56 days (Coulomb)		1385 1578	1493 1521	1751 1748	1635 1623
First cracking (days)		30	18	19	14
Compressive strength (psi)	3 days	3376	2866	2349	3085
	7 days	4339	3861	3264	4339
	28 days	5573	5032	4339	5494
	56 days	6130	5000	4737	6123

The following conclusions can be drawn from Phase I of the study:

- The ratio of water to cementitious materials has the most significant effect on chloride permeability;

- The permeability is not strongly correlated to the total air entrainment;

- The time for the first cracking to occur is related directly to the cement content and thus the strength of concrete;

- Class F fly ash is better than Class C fly ash in improving both the chloride permeability and cracking resistance of concrete;

- A proper increase of coarse aggregate can improve the permeability, the cracking resistance, and 28-day strength of concrete.

2.4   Phase II Study

The Phase II study was focused on Mixes 4-2, Mix 7, Mix 8, and Mix 14 shown in Table 2.1. Some important influential parameters on concrete properties that had not been examined in Phase I were studied in Phase II, including the type of fly ash, curing time, and aggregate gradation.

In addition to the selected mixes from Phase I, more mix designs were incorporated into the Phase II study, including two mix designs from Lafarge (the material supplier for the construction project at I-225 & Parker Road), and two mixes from CDOT - Class DT, and Class SF. Class SF was further modified for the application in the thin overlay on bridge decks. Some of the test results of the Phase II study are summarized in Table 2.2.

Table 2.2 – Some of Mix Designs and Test Results of the Phase II Study

		II4-4	II 8	SFSP-F
Cement content (lb/yd^3)		465	485	490
Fly ash lb/yd^3 (wt. % of cement)		F116 (25)	F97 (20)	F98 (20)
Silica fume lb/yd^3 (wt.% of cement)		18.6 (4)	19.4 (4)	19.4 (4)
W/(C+M)		0.37	0.41	0.41
Sand (lb/yd^3)		1231	1398	1340
Gravel (lb/yd^3)		1780	1595	1595
HRWR (oz/100 lb cement)		11.91	11.14	5.13
Micro Air (oz/100 lb cement)		0.54	1.6	0.82
Retarder (oz/100 lb cement)		2.16	3.2	2.05
Slump (inch)		6.0	5.5	4.5
Air content (%)		5.5	8.5	7.0
Permeability at 28 days (Coulomb)		3290 2747	2941 3161	4392 4141
Permeability at 56 days (Coulomb)		2528 2005	1393 1609	2212 2346
First cracking (days)		18	14	15
Compressive strength (psi)	3 days	3487	2512	3105
	7 days	4363	3695	3583
	28 days	5645	4657	4634
	56 days	6661	5414	5541

9

The following conclusions can be drawn from Phase II of the study:

- Class F fly ash is better than Class C fly ash in improving both the chloride permeability and cracking resistance of concrete.

- A proper increase in the content of coarse aggregate can improve the permeability, the cracking resistance, and 28-day strength.

- Increase in the proportion of an intermediate size of gravel does not improve the cracking resistance of concrete, nor the permeability. A larger size and higher proportion of gravel should be used.

- Longer curing time (12 days) seems to have an unfavorable effect on cracking resistance of concrete, but this need to be confirmed by a more detailed experimental study.

2.5   Selection of the Best Mixes

Considering the overall performance of the concrete mixes tested, a desired range of values for the concrete mix design parameters can be determined. The desired range for cement content is from 465 to 485 lb/yd^3; water/cementitious ratio from 0.37 to 0.41; and Class F fly ash from 20% to 25%. Recommended curing time is seven days.

Two mix designs are recommended for use in the summer and in the winter, respectively. In the summer season, Mix II4-4 is preferable. It has a low cement content of 465 lb/yd^3 and a high fly ash content of 25% of cement by weight. The water/cementitious material ratio can be slightly increased if necessary to improve workability. In the winter season, Mix II8 is preferable. It has higher cement content and lower fly ash content than Mix II4-4. In Mix II8, gravel content could be increased to 1780 lb/yd^3 and w/c could be slightly reduced. In both mixes, Class F fly ash should be used.

For the thin overlay concrete, Mix SFSP-F, II4-4, or II8 can be selected. If Mix II4-4 or II8 is used for thin overlays, smaller aggregate should be used in the mix.

2.6   Summary and Overall Accomplishments

Compared with Class DT, the concrete mixes developed in this study are more crack resistant and have higher fly ash content with the cement content reduced from above 600 lb/yd^3 to below 500 lb/yd^3. For the new mixes, the chloride permeability is reduced from about 6000 Coulomb (at 56 days) to below 2000 Coulomb. A narrow range of values are identified for the mix design parameters, which provide flexibility for small deviations in the mixes to meet specific needs. It is found in this study that Class F fly ash results in better durability performance than Class C fly ash.

3. The Behavior of FRP Reinforcement in Low Temperature Climates

3.1 Introduction

The effects of combined loading history and environmental exposure on the durability of carbon and glass fiber reinforced polymer reinforcement bars were investigated here (Cusson and Xi 2003). Specifically, the degradation of FRP bars due to coupled freeze-thaw cycling, tension, and fatigue loading was experimentally investigated. After a series of cyclic environmental preconditioning and mechanical loading, the degradation and the loading rate dependency of GFRP bars were evaluated from these aspects: strength degradation due to freeze-thaw cycling, static and dynamic tensile strength, elongation, Young's modulus, stiffness, fatigue strength, and failure modes including bar failures and grip failures.

3.2 Materials and Specimen Preparation

Two types of commercially available E-glass fiber reinforced polymer rods, and one type of carbon fiber reinforced polymer rod were selected in this study. One type of GFRP used is of the production line Aslan100 by Hughes Brothers, Inc. These glass-reinforced bars were made of continuous longitudinal E-glass fibers with 70% fibers by weight, and the fibers were bound by thermosetting vinyl ester (100%) resin matrix. The bars were wrapped with a clear helical glass fiber chord with the surface coated with resin and rolled in sand to provide enhanced bond properties. Hughes Brothers, Inc. differentiates between production lines by the color of the helical wrap. The bars used in this study are of the "clear" helical wrap. Two sizes of these bars were available for testing, 3/8-in diameter and 1/2-in diameter. These rough coated bars are denoted as 3/8"GFRP$_R$ and 1/2"GFRP$_R$, respectively. Another type of 3/8-in diameter E-glass fiber bars studied is C-Bar deformed FRP Bars manufactured by Marshall Industries Composites, Inc. These deformed bars were cast with a smooth clear urethane modified vinyl ester resin with "lugs" or protruded surface deformations. These surface textures provided a mechanical interlock to inhibit longitudinal movement when embedded in concrete. These bars consisted of 35% by volume binding material reinforced with 60% by volume continuous E-glass fibers. Approximately 3% ceramic fibers were included to reinforce the ribbed surface deformations.

The maximum average spacing of the ribs was 0.225 in, and the height of a rib was 0.030 in. A limited number of 1/2-in diameter bars of this type were also available. These bars with the smooth resin surface are denoted as 3/8"GFRP$_S$ and 1/2"GFRP$_S$.

Prestressing bars, with linearly oriented coal tar pitch-based continuous fibers, called Leadline, provided by Mitsubishi Chemical of Japan, were also included in this study. These were epoxy-impregnated 3/8-in nominal diameter carbon rods with a helical wrap nearly flush with the bar surface. Leadline is designed to be used as prestressing reinforcement. These bars contained 65% carbon fiber and 35% epoxy resin by volume.

The mean diameter and area of each type bar was determined. ASTM D3916 suggests a micrometer be used to measure the minimum and average bar thickness at "several points along its length." However, this method is impractical for the deformed and sand coated bars used in this study due to their irregular surface structure. Therefore, the average diameter of each bar was determined from the mass, length, and water displacement properties. The minimum and mean cross-sectional areas and diameters calculated for each specimen type are included in Table 3.1. Table 3.2 outlines the results obtained for each type material available.

Table 3.1 - Effective Diameter, Area, and Density of Test Specimens

Bar Type	DIAMETER (in)		AREA (in^2)		DENSITY	
	Minimum	Average	Minumum	Average	(g/cm^3)	(lb/in^3)
3/8" CFRP	0.359	0.369	0.101	0.107	1.744	0.063
3/8" GFRPs	0.369	0.388	0.107	0.118	1.947	0.070
3/8" GFRPr	0.376	0.390	0.111	0.119	2.046	0.074
1/2" GFRPr	0.503	0.515	0.199	0.208	1.999	0.072
1/2" GFRPs	-	0.5[1]	-	0.196[1]	-	-

[1] Samples were not available for this type bar to determine precise values.

Table 3.2 - Specific Gravity of Test Specimens

Bar Type	WEIGHT		SPECIFIC GRAVITY	
	(lb/ft)	(g/mm)	Minumum	Average
3/8" CFRP	0.084	0.118	1.70	1.74
3/8" GFRPs	0.096	0.147	1.85	1.95
3/8" GFRPr	0.108	0.158	1.92	2.05
1/2" GFRPr	0.180	0.271	1.89	2.00
1/2" GFRPs[1]	-	-	-	-

[1] Samples were not available for this type bar.

Since high compressive stresses and mechanical damage can occur due to surface serrations of traditional wedge-shaped grips, the FRP bars used cannot be tested using the same gripping techniques used for steel. For the experiments in this study, MTS 647.50 hydraulic wedge grips were used. Hence, it was necessary to encase the ends of the FRP specimen in an anchorage system to distribute the grip stresses so they were not concentrated at critical points on the bar. An accurately designed anchoring device must be able to develop the full strength of the bar allowing for failure to occur within the gage length of the specimen. Initially, bars were cut 40 inches in length, however, due to coupled loading and conditioning restraints, maximum specimen length was limited to 24 in, independent of bar diameter. The free-length is the unsupported distance between the end anchorage grips. The average free-length for the 40-in specimens was 16 in, and the 24-in samples had an average free-length of 11.34 in. The tubular anchorage system developed for this project requires each end of the reinforcing bar be embedded into an RB4-40 (Schedule 40) Steel Pipe with Randustrial M-183 Bolt Anchor Immersible Sulfaset expanding cement filler.

To ensure the bar will not pullout from the tube when loaded, an adequate embedment length needs to be established. Due to the restriction on specimen length, the maximum embedment lengths for the 40-in and 24-in specimens ranged from 24 to 32 times and 12 to 16 times the bar diameter, respectively. The free-length-to-diameter ratios for the bars vary from 24-43 depending on bar size. Initial tensile tests showed these lengths to be sufficient for GFRP

specimens; however, the anchorage system for CFRP samples needed to be redesigned. Therefore, a limited number of CFRP and GFRP samples were made with anchorages filled with epoxy. The epoxy grips were assembled in a similar manner as described previously.

3.3   Experimental Procedures

An environmental chamber was used to test the influence of sub-zero ambient temperatures on the mechanical and visco-elastic properties of the FRP rods. The intent of this study is to consider short-term axial tension for ultimate strength, Young's modulus, and elongation obtained at ambient temperature and $-20°F$ (-29°C) with a tolerance maintained within $\pm3°F$.

An extensive review on previous experiments on temperature effects of FRP reinforcements showed that there seemed to be a lack of abundant data for FRP in the low temperature range between $-20°F$ to $60°F$. Each specimen requiring pre-conditioning was thus subjected to low temperature thermal cycling between $68°F$ (20°C) and $-20°F$ (-29°C) temperature excursions with a 1-hour hold at $-20°F$ and 20-minute hold at $68°F$, achieving an 8 cycle per day rate. Specimens were exposed to 250 freeze-thaw cycles corresponding to 750 hours of exposure. A total of 105 bars were prepared, thirty-two of which were pre-conditioned in this manner: 1-40"-long 3/8" CFRP sample, 15-3/8"GFRP$_S$, 4-3/8"GFRP$_R$, 11-1/2"GFRP$_R$, and 1-1/2"GFRP$_S$. Specimens that were not subjected to freeze-thaw cycling were stored in the structures testing laboratory at room temperature and relative humidity.

Following 250 thermal cycles, the bars were visually examined for the development of cracks and long-term mechanical properties were then investigated. Investigations were made into the variable rate effect on the ultimate tensile strengths and elastic properties of the different FRP reinforcements. Preliminary fatigue tests were performed to establish a definitive program for future study to determine the relationship of load range to number of cycles, and effect of micro-cracking endured during freeze-thaw cycling.

A minimum of three specimens were considered for each test and environmental combination. In many cases, several samples were available for testing in each category, with

improper failure modes eliminated from the cumulative results.

The static tension tests followed the guidelines set forth in ASTM: D 3916, Standard Test Method for Tensile Properties of Pultruded Glass-Fiber reinforced Plastic Rod. Similar methods can be applied to the evaluation of carbon fiber bars, but may not be adequate at the high level of stress required for tensile failure.

After initial static tensile tests were completed, fatigue tests were designed at 80% of what was believed to be the average ultimate strengths of the reinforcement bars tested. Concern was raised after initial fatigue tests did not fail after 1,000,000 cycles. After a careful investigation into the reasoning behind this phenomenon, the rate dependency of glass-fiber FRP reinforcement was made apparent. Unlike carbon and aramid fiber FRP bars, the strength of glass fiber bars is strongly rate dependent; as the loading or strain rate increases, tensile strength increases.

Past research into fatigue properties of fiber composites has often focused on high modulus carbon and aramid fiber bars. However, it is important to realize that composite materials containing E-glass fiber reinforcement tend to be much more sensitive to tensile or cyclic fatigue loading in the fiber direction than composites reinforced with other fibers. The effect of loading frequency on the mechanical properties of most continuous carbon FRP products appears to be negligible when tested in the longitudinal direction parallel to the reinforcing fibers. Properties of glass fiber polymer reinforcements, on the other hand, have shown a significant rate dependency. It is also apparent that there are no conclusive reasons for this phenomenon.

Initial tension tests were performed using a Tinius Olsen testing apparatus and produced failure times corresponding to one half-cycle at loading rates of 0.1 in/sec, 1.0 in/sec and 10 in/sec would occur at approximately 5.0, 0.5 and 0.05 seconds respectively. Samples from three of the different type bars available, 3/8"$GFRP_S$, 3/8"$GFRP_R$, and 1/2"$GFRP_R$, were investigated in this manner.

The initial intention of the study was to investigate a strength comparison between three

16

loading frequencies at 0.1 Hz, 1.0 Hz and 10 Hz using the MTS dynamic testing machine. In an attempt to obtain 1/2-cycle ultimate strength failures with the MTS machine at times corresponding to maximum possible frequencies, several loading programs were considered. These initial tests were performed in load control, both as a ramp rate in lbs/sec, and as frequency, in Hz (cycles/sec). It was then realized that better performance results were realized by application of stress in stroke control, applied as a ramp rate in in/sec of displacement. It was established that for these particular tests the machine was only providing consistent loading frequencies up to a maximum of 2 Hz. Therefore, loading frequencies of 0.1 Hz, 1.0 Hz and 2 Hz were ultimately used. Between the two loading machines' control application methods, the quickest failure observed still only occurred at 0.20 seconds. Data was thus accumulated for a series of specimens at 2 Hz rather than 10 Hz as initially planned. Detailed information regarding loading rates are included in the full report.

3.4 Experimental Results and Discussions

3.4.1 Static Tension Results

Several comparisons were made with the data collected from the ultimate tensile strength tests performed on the Tinius Olsen machine. The average ultimate tensile strength for each type bar was established.

The descriptions of each bar are coded as follows.

0.38GS-1u = (bar diameter)(fiber type)(surface texture)-(# this type bar)(unconditioned)

For example, 0.38GS-2u stands for the second unconditioned 3/8"-dia smooth surface glass fiber bar tested.
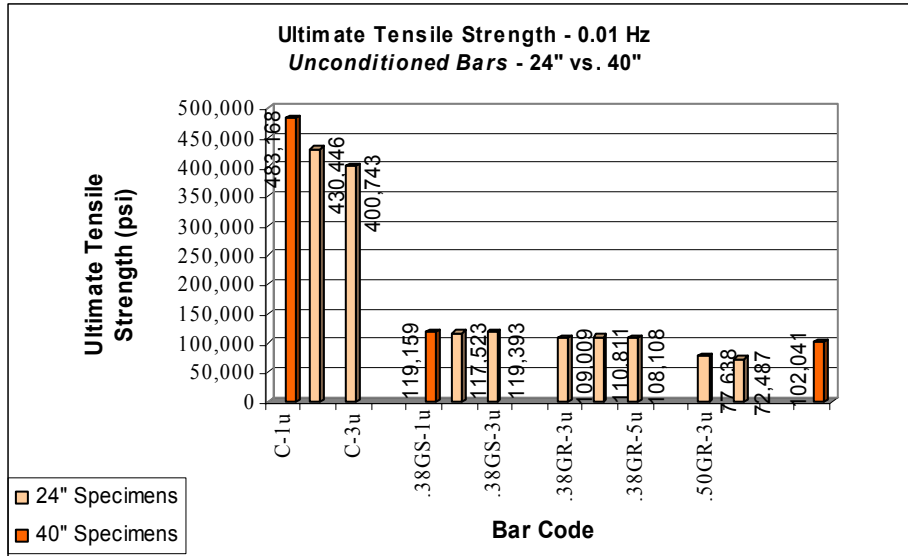
Ultimate Tensile Strength - 0.01 Hz
Unconditioned Bars - 24" vs. 40"

Figure 3.1 - Results of Initial Tensile Tests for Unconditioned Specimens

Ultimate Tensile Strength - 0.01 Hz
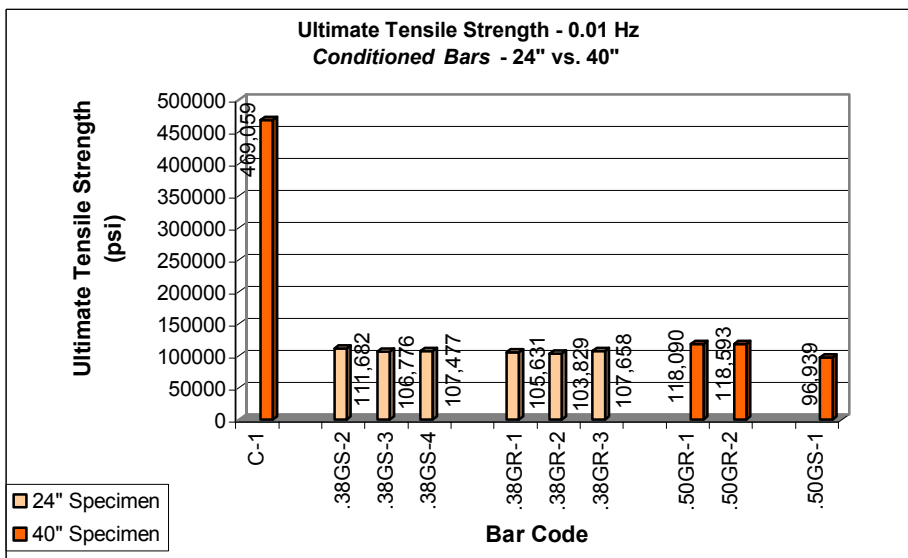*Conditioned Bars - 24" vs. 40"*

Figure 3.2 - Results of Initial Tensile Tests for Conditioned Specimens

It was intended to examine the variability of test results between the 40-in and 24-in specimens to determine whether the free-length or grip length of the test specimen has an effect on the outcome. Figures 3.1 and 3.2 graphically compare the results obtained for each 24-in and 40-in specimen, unconditioned and conditioned, respectively. However, there were not enough

18

40-in specimens tested to arrive at an adequate conclusion. In most cases, the ultimate strengths of the 40-in specimens were found to be higher than the average strengths of the 24-in bars. This was not the case in all of the tests; discrepancies could be due to variability in loading rate. Preliminary results show that the average strength of the 40-in unconditioned CFRP bars is 483,168 psi, a 14% greater ultimate strength than the 24-in unconditioned CFRP bars. The average ultimate tensile strength of the carbon fiber bars are about 4-times higher than that of the glass fiber bars. The average strengths of the 24-in and 40-in unconditioned 3/8" $GFRP_S$ specimens were 118,458 psi, and 119,159 psi, respectively. The average strength of the 24-in unconditioned 3/8" $GFRP_R$ specimens was 109,309 psi.
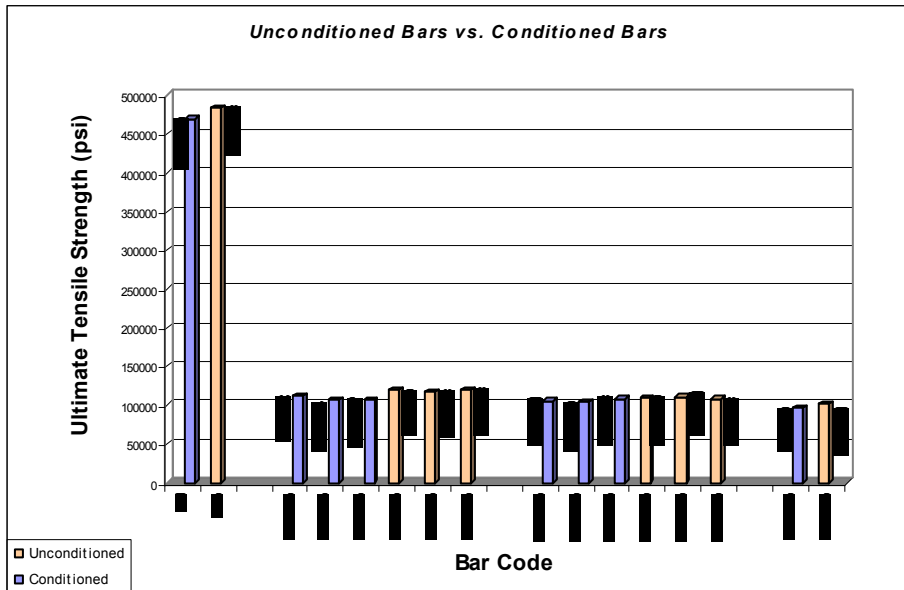

Figure 3.3 - Comparison of Results of Initial Tensile Tests

Another comparison considers the average ultimate tensile strengths of unconditioned versus conditioned specimens. Figure 3.3 graphically compares the tensile strengths obtained from the tested unconditioned and conditioned bars. For unconditioned specimens, initial tests showed that the 3/8"$GFRP_S$ rods (average strength of 118,692 psi) had a slightly higher strength capacity than the 3/8"$GFRP_R$ (average strength of 109,309 psi) and 1/2"$GFRP_R$ (average strength of 75,063 psi). Each of these bars experienced failure within the gage length, with no slippage within the anchorage. However, full distribution of stresses in the 3/8-in specimens was not

realized before failure since several of the specimens in this group had hard cores remaining. The 1/2"GFRP$_R$ bars tested at this loading rate experienced considerable fiber failure, but a greater cross-sectional area reduces its ultimate strength comparatively.

For glass fiber bars, the 3/8"GFRP$_S$ specimens realized the greatest reduction of strength between unconditioned and conditioned bars tested. The average ultimate strength of these conditioned GFRP bars decreased by nearly 10,000 psi, an 8% reduction in strength. The average ultimate strength of the conditioned 3/8"GFRP$_R$ bars was found to be approximately 3,600 psi lower than the tested unconditioned specimens, a 3% decrease. The ½"GFRP$_S$ bars also showed similar results, with a 5% decrease in strength noticed in the conditioned specimens.

Figure 3.4 - Unconditioned CFRP Grip Failure

The most valid results for considering tensile strength are obtained from specimens in which failure occurs in the free-length of the bar. In the initial tests, all carbon fiber bars exhibited failure near or within the cement casing of the grips. Initial unconditioned CFRP bars tested experienced complete fracture at the grip surface. In some unconditioned specimens, the fibers began to fray within the free-length before failure occurred due to pullout. Damage to the steel tube grips illustrated the effects of the strong lateral pressures required to hold on to the carbon fiber specimens at high tensile loads.

Figure 3.4 shows the failure of the carbon fiber bars near the grips. The cement binder did not provide adequate bond strength to prevent pullout from the anchorage before failure in the free-length of the specimen could occur. A supplementary anchorage system was designed using epoxy.

3.4.2 Failure Mode Analysis under Dynamic Tension Tests

A JVC digital video camera was used to capture failures of a group of samples for each loading rate. The failure modes of ten 3/8"GFRP$_S$ specimens were analyzed in this manner. This procedure aided in the visual inspection of the failure modes. Each clip could be slowed down in order to record such aspects as: which grip initiated failure, was fiber failure gradual or instantaneous, how many bursts of failure did the sample endure before complete fracture, etc.

A fiber-break propagation model infers that as each fiber breaks, the redistribution of stress leads to additional stress on neighboring fibers. This process was visually evident upon examining the filmed failures. As the specimens were loaded, outer diameter fibers would initiate failure. Often, initial fiber breaks occurred at the surface of the anchorage grip. Fiber breakage accumulated rapidly, often accompanied by bursts of energy release causing total fiber failure. In several cases, when the ultimate strength was reached and the load capacity returned to zero, a hard center core of fiber/matrix material remained. Although bars tested at higher frequencies registered greater strengths, it was apparent that these bars failed in tension before the stress could be distributed throughout all fibers of the cross-section. Bars tested at 0.1 Hz loading performed better in this manner and experienced a greater number of fiber breaks. For the 3/8-in diameter specimens tested at 0.1 Hz, 5 out of 7 experienced nearly complete fiber failure, with the bar being completely severed in two.

There were significant differences noticed between bars of different cross-sectional diameters. The 1/2-in diameter GFRP specimens tested at low frequencies experienced several bar pullouts from the anchorage system. Since the chemical bond between the concrete filler and the FRP bar is extremely low, mechanical interlock becomes the primary means of stress transfer. The lack of this mechanical interlock would seem to explain the majority of bar pullouts in the sand coated 1/2"GFRP$_R$ specimens. All grip slippages of this size

occurred in the top grip. In response to the number of bar pullouts that were experienced in the 1/2"GFRP$_R$ specimens with the cement anchor system, a series of additional tests were performed on these type bars with epoxy grips. Although the epoxy grips did provide comparable strength values, all of these bars pulled out of the epoxy grips. Several of the 1/2"GFRP$_R$ specimens also experienced severe fiber-matrix debonding in the grip region. It is apparent that for these bars, the ultimate strength was not reached before the fiber-matrix interfacial bond strength was exceeded.

Figure 3.5 - Failure Mode of 1/2"GFRP$_R$

Figure 3.6 - Failure Mode of 3/8"GFRP$_S$

Unlike the previous responses exhibited by the ½-in diameter bars, all of the bars pre-conditioned in freeze-thaw cycling, experienced complete fiber failure. These failures are shown in Figures 3.5. Still, overall, the conditioned strengths were less than those realized in unconditioned specimens. Nearly all 3/8"GFRP$_S$ specimens experienced complete bar failure. The common failure mode is shown in Figure 3.6. The 3/8"GFRP$_S$ bars were the only type tested that did not experience any pullouts of the bar from the anchorage. A couple of these type of bars did, however, experience shearing of the fiber-matrix interface in the grip region. This was common among 3/8-in diameter bars; 50% of those tested at 1 Hz to 2 Hz experienced this

failure mode.

The 3/8"GFRP$_R$ bars were pulled out of the epoxy filled anchorages. Although the epoxy filled grips realized equal if not greater strengths than the grout filled grips, all of the bars tested with the epoxy grip system experienced bar pullout.

3.4.3   Variable Rate Tension Results

The rate sensitivity of the glass fiber strength is quite apparent in comparing the ultimate strength results obtained with various loading or frequency rates. Figures 3.7 – 3.9 visually illustrate the strong load rate dependence of each type bar. Figure 3.10 shows the overall rate dependant trend of each bar type considered.

Static tensile strengths measured with the Tinius Olsen machine are significantly less than those recorded at fatigue rates. And although the data obtained from the static tests does follow the trend of load rate increase, the correlation of test results obtained from different types of machines is very poor (which is consistent with the results obtained by other researchers). Freeze-thaw pre-conditioned specimens experienced at least a 3% decrease in strength in all cases, except for the 3/8"GFRPs loaded at 2 Hz (Figures 3.11-3.14). Due to the fact that there were only 2 unconditioned samples available for testing as opposed to 4 conditioned specimens, it is supposed that if the sample number increased for the unconditioned case, a similar trend would be evident. Among all types of bars considered, the greatest ultimate strengths were realized by the 3/8"GFRPr. No definitive conclusions can be made on whether load control or stroke control produces greater ultimate strengths. Stroke control has been seen to provide better failure modes and repeatable stiffness curves.
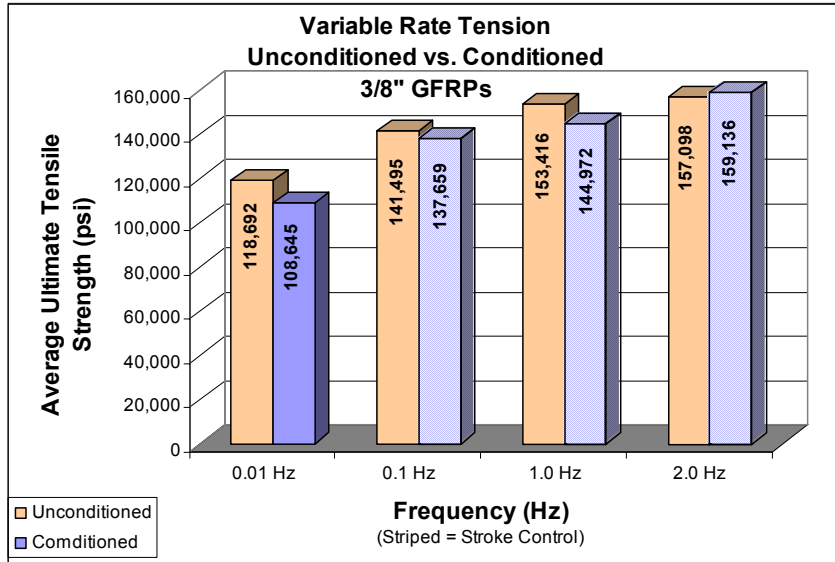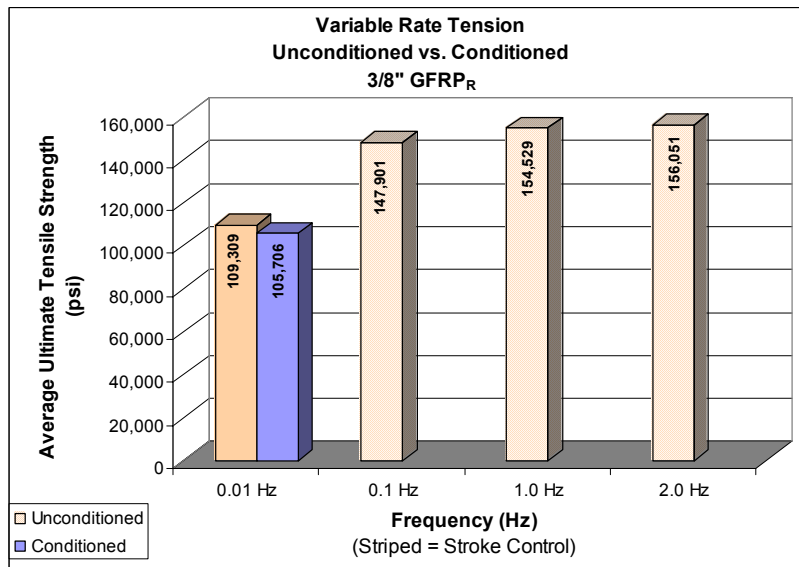
Figure 3.7 - Variable Rate Tension 3/8" GFRP$_S$

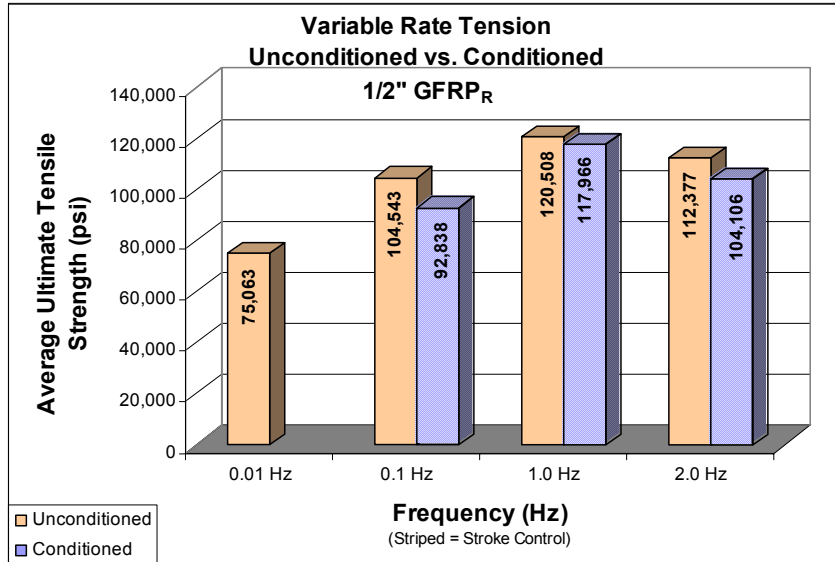Figure 3.8 - Variable Rate Tension 3/8" GFRP$_R$

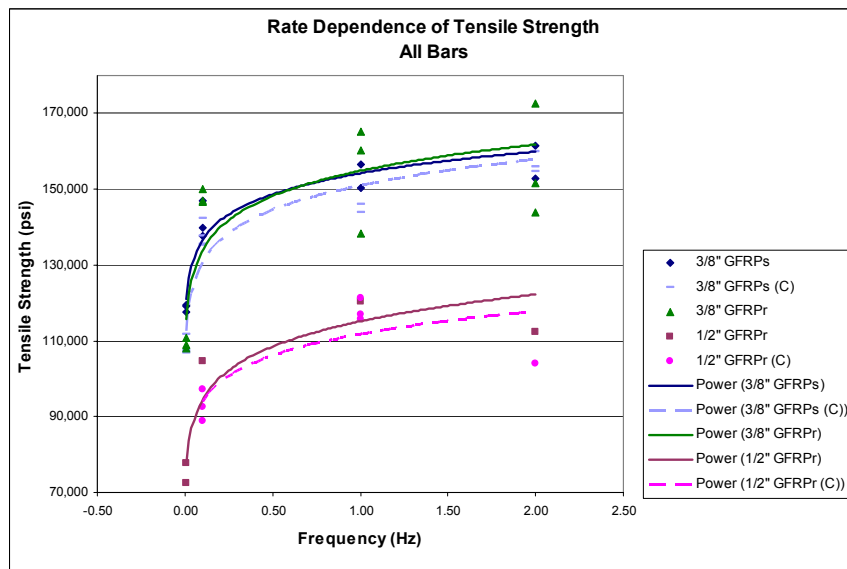Figure 3.9 - Variable Rate Tension 1/2" GFRP$_R$

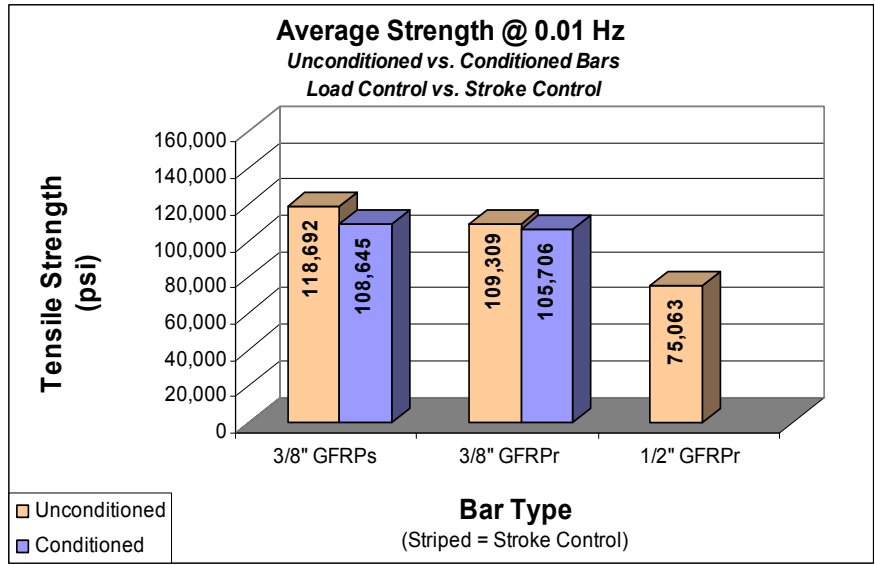Figure 3.10 - Rate Dependence of Glass Fiber Reinforced Polymer Bars
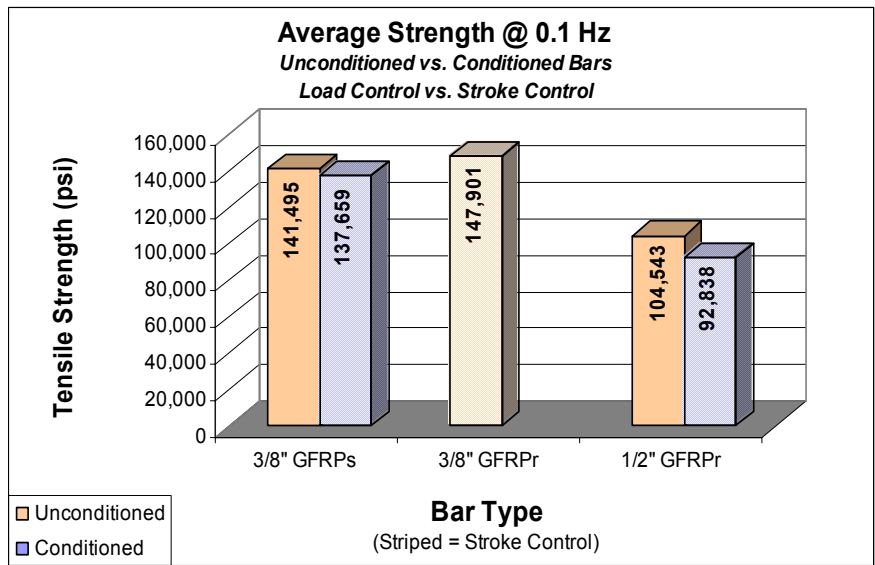
Figure 3.11 - Average Strength at 0.01 Hz

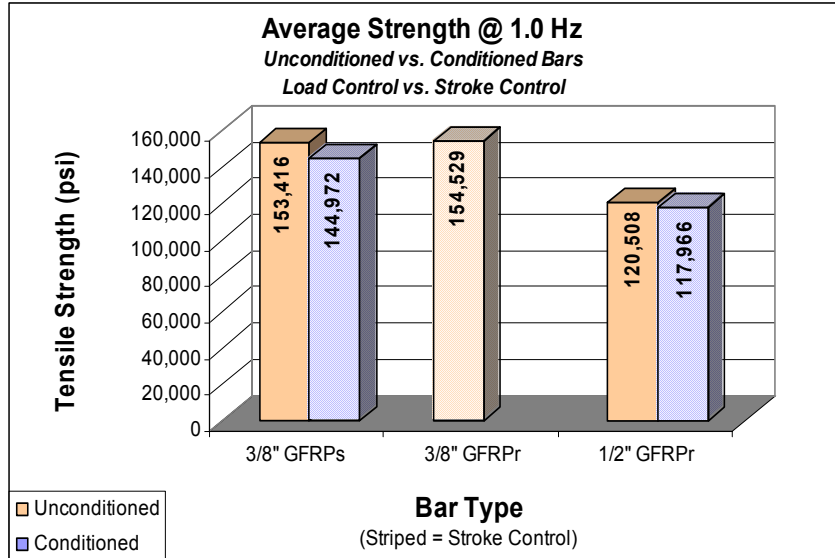Figure 3.12 - Average Strength at 0.1 Hz

Average Strength @ 1.0 Hz
Unconditioned vs. Conditioned Bars
Load Control vs. Stroke Control

Tensile Strength (psi)

	3/8" GFRPs	3/8" GFRPr	1/2" GFRPr
Unconditioned	153,416	154,529	120,508
Conditioned	144,972		117,966

160,000
140,000
120,000
100,000
80,000
60,000
40,000
20,000
0

Bar Type
(Striped = Stroke Control)

☐ Unconditioned
☐ Conditioned

Figure 3.13 - Average Strength at 1.0 Hz

Average Strength @ 2.0 Hz
Unconditioned vs. Conditioned Bars
Load Control vs. Stroke Control

Tensile Strength (psi)

	3/8" GFRPs	3/8" GFRPr	1/2" GFRPr
Unconditioned	157,098	156,051	112,377
Conditioned	159,136		104,106

160,000
140,000
120,000
100,000
80,000
60,000
40,000
20,000
0

Bar Type
(Striped = Stroke Control)

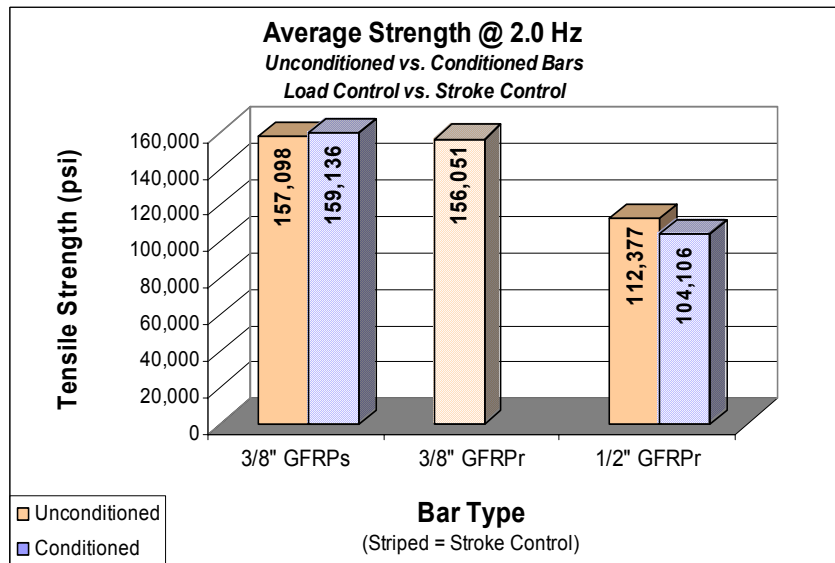☐ Unconditioned
☐ Conditioned

Figure 3.14 - Average Strength at 2.0 Hz

3.4.4   Elastic Modulus

Several factors can affect the elasticity of fiber reinforced products. The elastic modulus of glass fiber polymer rods subjected to variable rate tension tests was evaluated for each rate of

27

loading.   Specimens were loaded uniaxially, and load and displacement data was recorded continuously until failure.   Data was acquired at increments of 0.005 to 0.0005 seconds depending on the predicted time to failure.   Most of the tests resulted in a load-displacement relationship linear up to failure as shown in Figure 3.15.   In these cases, sudden failure resulted in rapid unloading of the specimen.
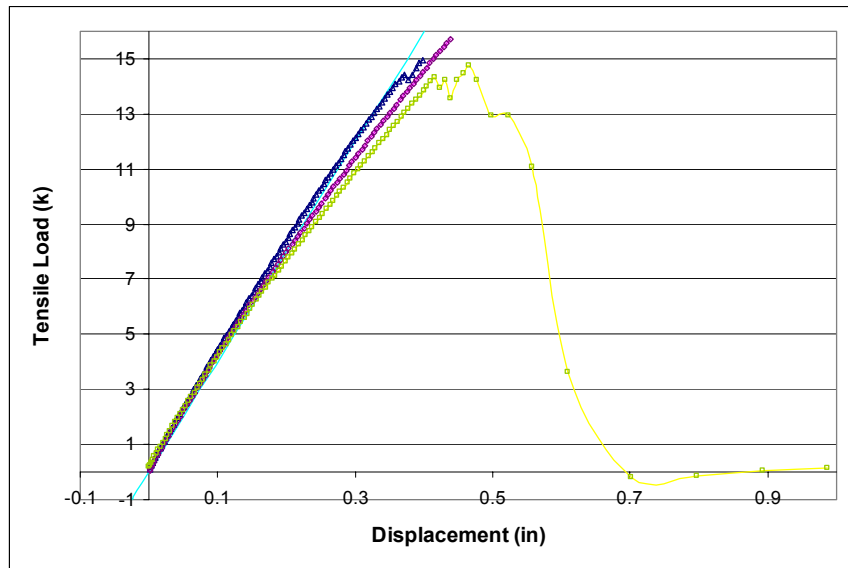

Figure 3.15 - Linear Elastic Behavior to Failure

The linear portion up to failure was considered in calculating the elastic modulus. The axial stress for each data point was calculated by dividing the load value by the specimen's original cross-sectional area.   The average initial cross-sectional area within the gage length of the specimen was used for this calculation.   Strain values were calculated similarly by dividing displacement values for each data point by the original length of the specimen.   Other load-displacement relationships indicate that after ultimate strength was achieved, response leads into a non-linear region of cyclic load reductions. Figure 3.16 illustrates several samples exhibiting this behavior.   Stress-strain curves and load-displacement stiffness curves were drawn for each set of loading frequencies, as well as for each bar type. Young's modulus was calculated based on the least squares method and least squares regression lines were generated. The stress-strain diagram is shown in Figure 3.17. Stiffness values of fiber reinforced polymers are usually in the

range of 1/5 to 2/3 that of steel (29 x 10^6 psi). The least-square load-displacement curve for each set of specimens was also calculated and illustrated in Figure 3.18.
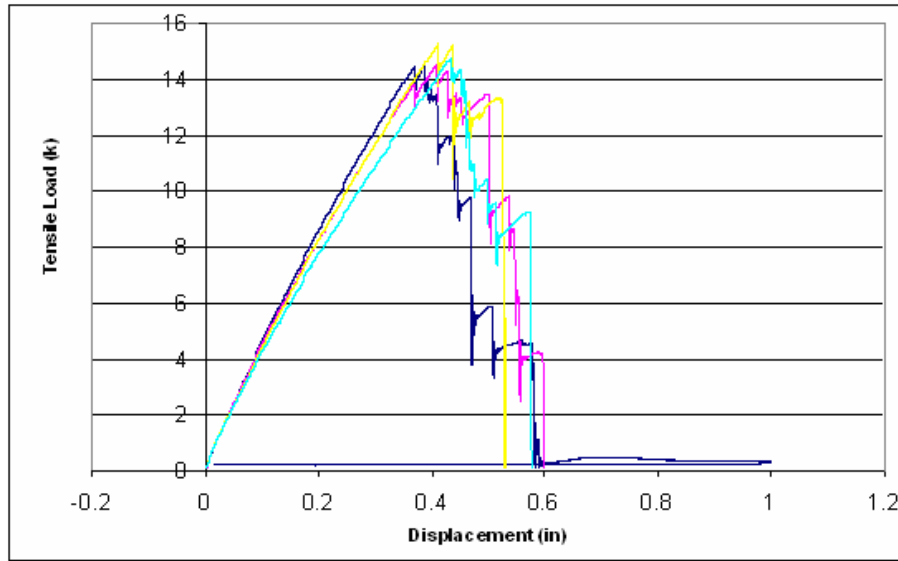

Figure 3.16 - Linear Behavior with a Non-Linear Region of Cyclic Load Reductions after Failure
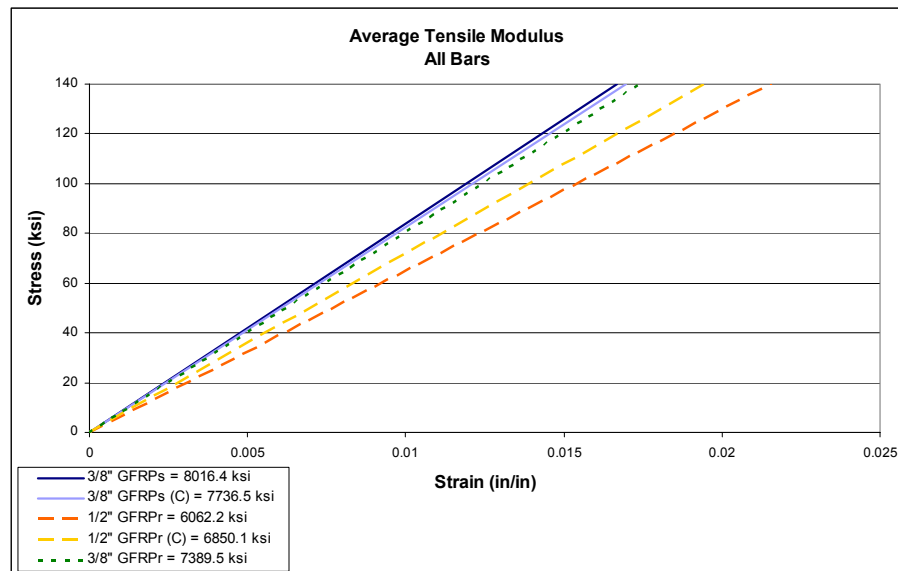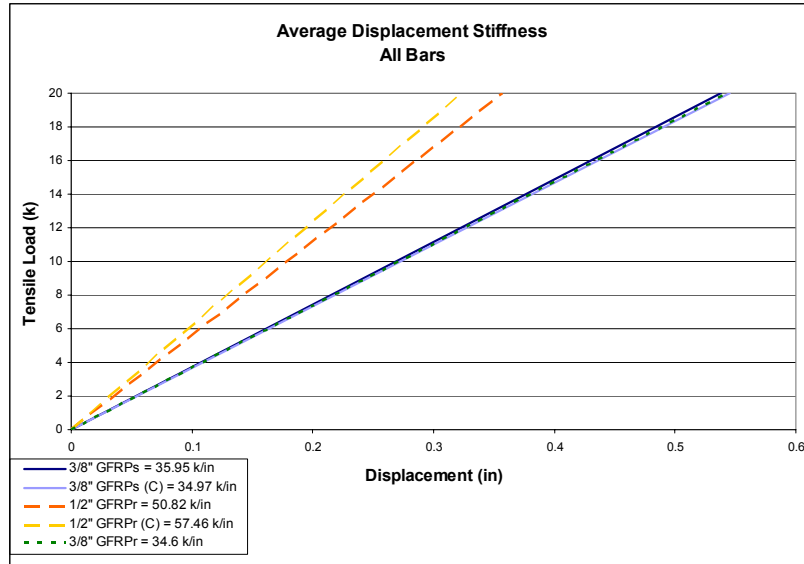

Figure 3.17 Average Tensile Modulus

Figure 3.18 - Average Displacement Stiffness

3.4.5 Fatigue Tests

Generally, fiber reinforced polymer bars tend to exhibit good fatigue resistance. Many variables can ultimately affect the total number of cycles to failure: stress levels, stress rate, mode of cycling, process history, material composition, and environmental conditions.

Fatigue tests were carried out with an MTS 110-kip servo hydraulic testing machine. Initial tests were designed to apply fatigue loading cycles at a test frequency of 5 Hz repeated 2-million times on specimens maintained at –20°F (-4ºC). These results were to be compared to those at room temperature to determine the effect of low temperature on endurance limit. In preliminary tests, the MTS machine was used in load control. In this method, as the test material was damaged in fatigue, greater displacements resulted.

The post fatigue performance of three 1/2"GFRP$_R$ bars was investigated. When the failure of the tested specimens did not occur after a specified number of cycles, the static strength was measured. The first two examples are 3/8"GFRP$_S$ specimens cycled at 5 Hz between 40%-50% of the expected ultimate strength. The first of these successfully completed 985,000 cycles before power was lost in the laboratory. The residual strength of this test specimen was found at

30

0.01 Hz to be 137,346 psi. The second specimen was cycled at 5 Hz repeated 765,374 times. The recorded residual strength of this bar at 0.01 Hz was 122,252 psi. The third trial was a 3/8"GFRP$_R$ specimen cycled at 5 Hz at roughly 20-25% of its ultimate strength. This bar was removed after 500 cycles and tested to have a remaining strength of 154,505 psi at 2 Hz. In each of these cases, load capacity was not significantly reduced. Static strength should be reduced with increasing number of cycles. However, the failure of the FRP bars will not occur if cycled at less than 60% of their ultimate strength.

3.5   Summary and Conclusions

Two types of commercially available GFRP reinforcing bars (3/8"GFRP$_S$, and 3/8" & 1/2"GFRP$_R$) and one type of CFRP bars were studied in the project. A total of 105 bars were prepared, 32 of the bars were pre-conditioned with low temperature thermal cycling at eight cycles per day. Specimens were exposed to 250 freeze-thaw cycles corresponding to 750 hours of exposure.   Following 250 thermal cycles, the bars were visually examined for the development of cracks and then static and dynamic tension tests were performed to determine the ultimate tensile capacities of the FRP bars. Preliminary fatigue tests were performed to establish a definitive program for future study to determine the relationship of load range to the number of cycles to failure, and the effect of micro-cracking endured during freeze-thaw cycling.

The effect of the rate of loading on the tensile strength properties of glass fiber polymer reinforcements was investigated in order to establish a basis for cyclic fatigue loading procedures. The following conclusions have been made based on the analysis of the test results:

- The rate sensitivity of the strength of glass fiber reinforcing bars was quite apparent.

- There were noticeable increases in strength and marked changes in fracture appearance with increased loading rate.

- Freeze-thaw conditioning did have some deleterious effect on the ultimate strength of glass

fiber polymer reinforcing bars.

- Stroke controlled tests produced more complete failure modes and repeatable load-displacement curves than load controlled tests.

- A basis for fatigue testing up to 2 Hz has been established.

- A complete experimental system and testing procedures are established for durability testing of FRP materials under environmental and mechanical loadings.

In order for FRP reinforcing bars to be successfully implemented in roadway construction projects, it is essential to develop a firm understanding of the durability properties of FRP bars and effects of exposure to severe and frequently changing environments. Preliminary results in this report show that freeze-thaw exposure may have some effects on the fatigue properties of FRP bars. The degree of deterioration of the FRP bars depends on the temperature ranges and number of freezing-thawing cycles applied. Under the temperature conditions applied in this study, the decrease of the tensile strength of the FRP bars was no more than 10%. Although the temperature conditions in the tests were more severe than the actual temperature fluctuations in Colorado, the degradation of the tensile strength should be considered properly in structural design.

# 4. Evaluation of FRP Prestressed Precast Panels

4.1 Introduction

This chapter summarizes a study that compared the strengths of precast panels and composite slabs that were prestressed with CFRP tendons and steel strand (Zyslstra et al. 2001). The strengths of bare panels as well as those constructed with the addition of a 5-in topping slab were investigated. Furthermore, a series of pullout tests were performed on Leadline CFRP tendons, seven-wire steel strand, C-BAR GFRP reinforcing rods, and #4 black steel bars to attain a better understanding of the bonding characteristics between these materials and concrete. The mechanical properties of the FRP bars are described in Chapter 3 of this report.

4.2 Pull-Out Tests

Pullout tests were conducted on 0.39-in (10-mm) diameter Leadline bars and 0.5-in (13-mm) diameter C-Bar rods. Furthermore, 3/8-in (9.5-mm) seven-wire strand and #4 (13-mm) deformed mild steel reinforcement were also tested for comparison purposes. A comparison of the pullout strengths of the Leadline bars and prestressing strand shows that Leadline consistently had higher bond strength. A total of five Leadline tests gave an average bond strength of 1.58 ksi while five steel strand tests gave an average bond strength of 0.99 ksi. The bar chart in Figure 4.1 summarizes the bond test results.

Making the same comparison for C-BAR and reinforcing steel, it can be inferred that C-BAR rods had a higher bond strength than steel bars. In this case, the results are only separated by a small difference. Three C-BAR tests with an embedment length of $5d_b$ gave an average bond strength of 3.15 ksi while the #4 bars gave an average bond strength of 2.9 ksi.
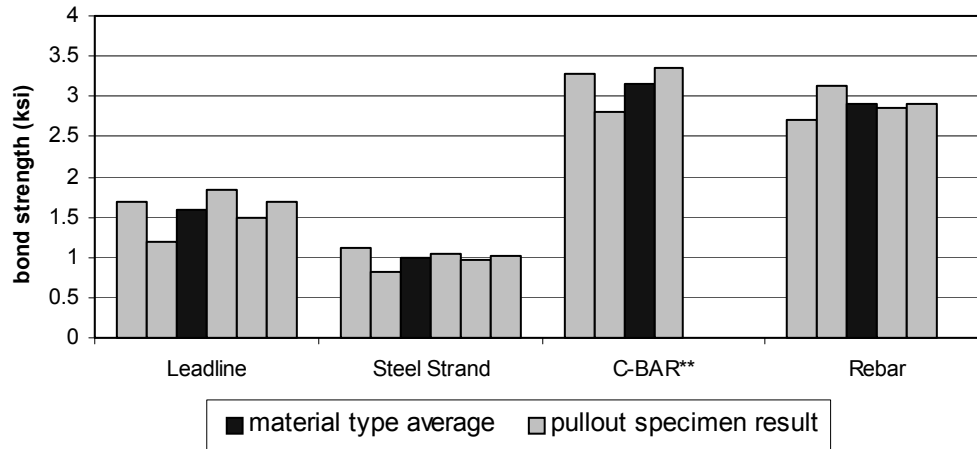
Figure 4.1 - Bond Strengths for Each Specimen in Pullout Tests

**5d$_b$ embedment length

4.3 Prestressed Panel Tests

A total of five prestressed panels were tested to failure. Three of them were tested as bare panels and the remaining two had composite topping slabs. The panels were designed using the 16th Edition of the AASHTO Specifications (AASHTO 1996) with additional considerations for CFRP tendons. The panels were 3.5- in thick, 116-in wide, and 96-in long.

Four of the panels were designed to satisfy the minimum requirements of AASHTO. They were prestressed with 14 tendons spaced symmetrically over the 96-in length. Perpendicular to the prestressing tendons, reinforcing bars were placed at 12-in spacing. Two of these were prestressed with 0.315-in (8-mm) Leadline CFRP tendons and reinforced with 0.5-in (13-mm) C-BAR GFRP reinforcing rods. The other two were prestressed with 3/8-in (9.5-mm) seven-wire, low relaxation prestressing strand and reinforced with #3 steel bars (9.5-mm diameter). A jacking force of 17 kips was used for both CFRP tendons and steel strands. The design is shown in Figure 4.2.

One panel from each set was tested as it was. The other panel fom each set had a 5-in

34

composite topping slab cast with one mat of #3 (9.5-mm diameter) steel reinforcing bars spaced at 12 inch in each direction. The steel reinforcement in the grid was fitted with strain gages to obtain load distribution data for the slabs. The design of the composite topping slab is shown in Figure 4.3.

A third panel type was also tested. This panel was designed by CDOT and used in the bridge at I-225/Parker Road. The CDOT panel had the same overall dimensions as the above tested panels. However, the reinforcement was considerably different. Each panel was prestressed with twenty 0.39-in (10-mm) diameter CFRP tendons spaced symmetrically over the 96-in length. GFRP reinforcing bars with a 0.5-in (13-mm) diameter were placed at 6-in spacing perpendicular to the prestressing tendons. The design is shown in Figure 4.4. Hence, the panel was more conservatively designed than the first four. It was based on a standard panel design used by CDOT. This design had been used for a variety of span lengths and is very conservative for the span length used in this project.

All panels had straight tendons with an eccentricity of 0.47 in. This eccentricity was required to provide an additional factor of safety for the construction loads with the given tolerance for the placement of the tendons.
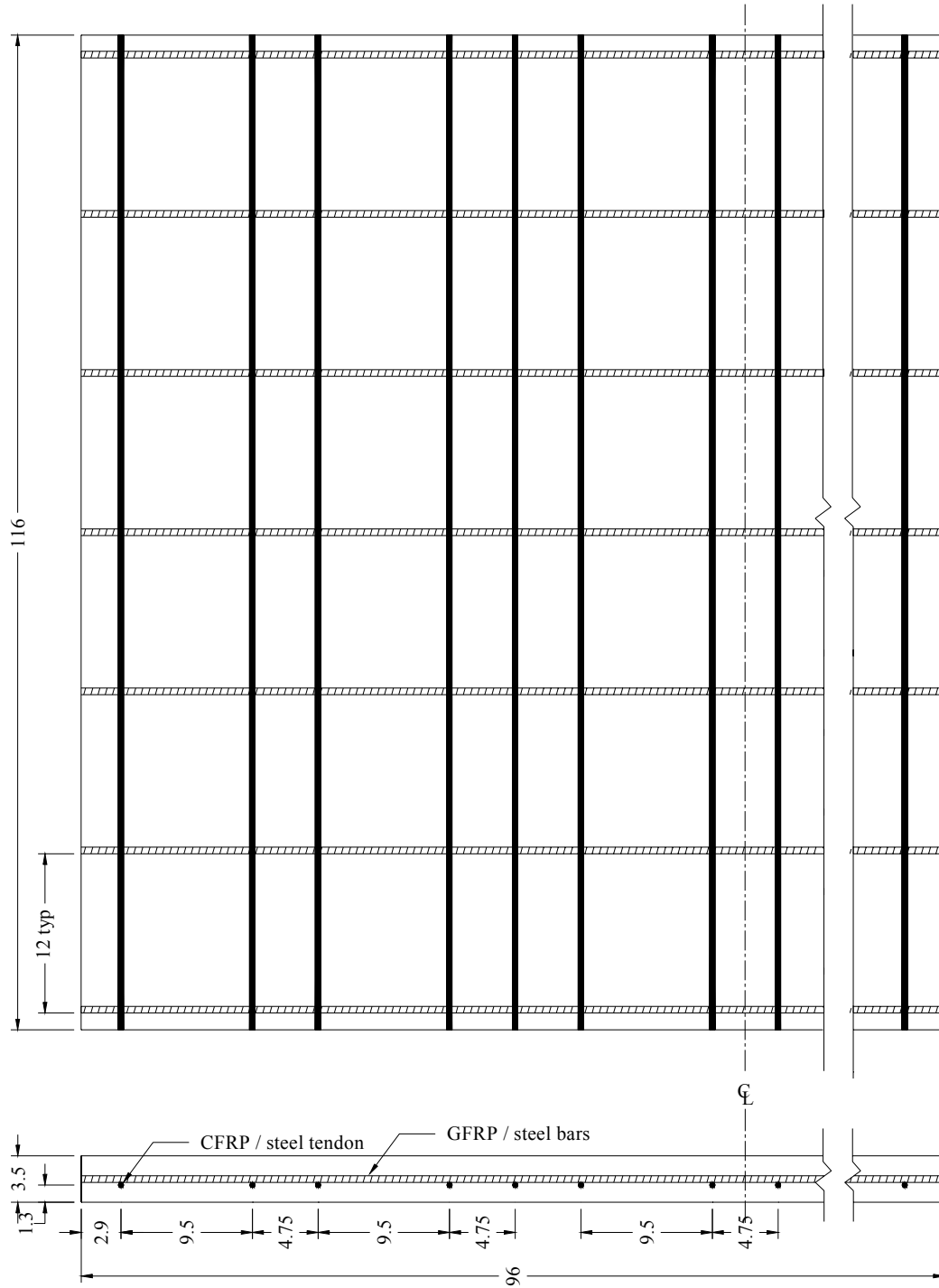
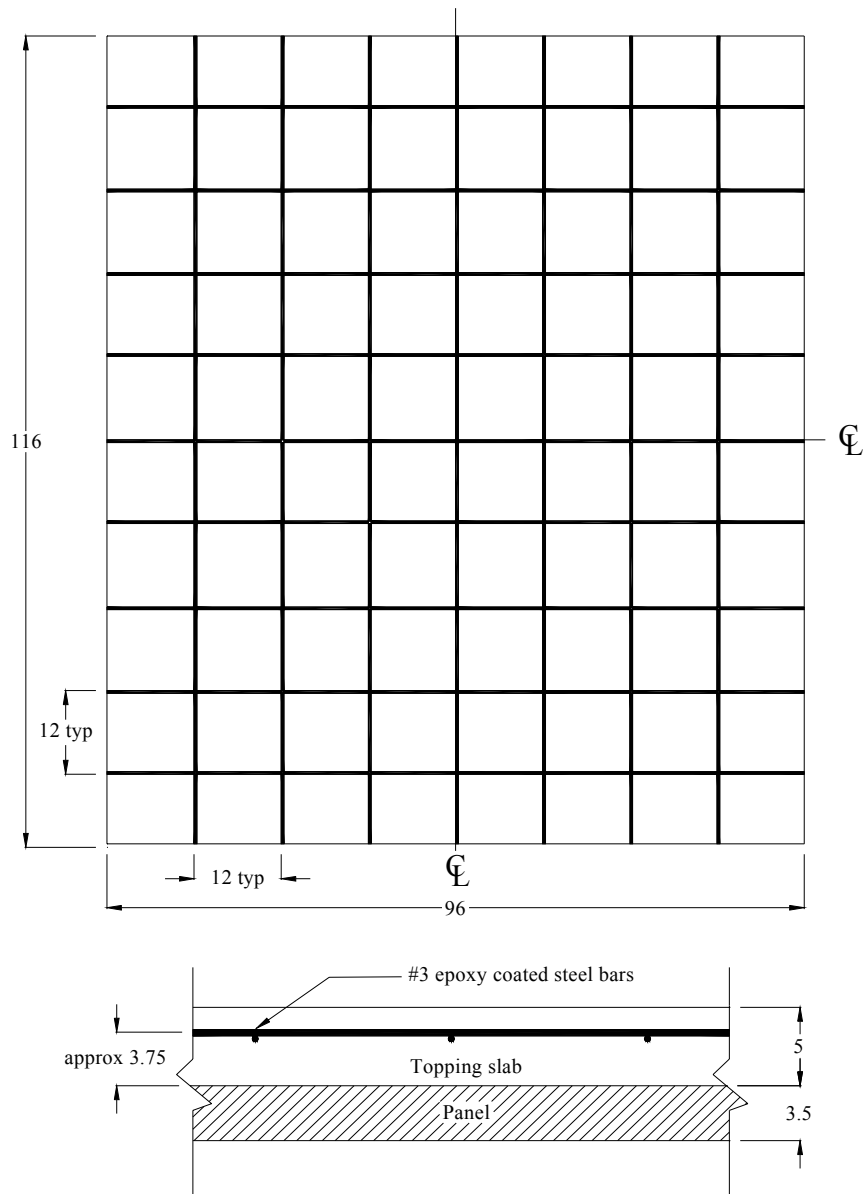Figure 4.2 - Cross-Section and Plan View of First Four Test Panels (all values in inches)

Figure 4.3 - Cross-Section and Plan View of Panel and Topping Slab (all values in inches)
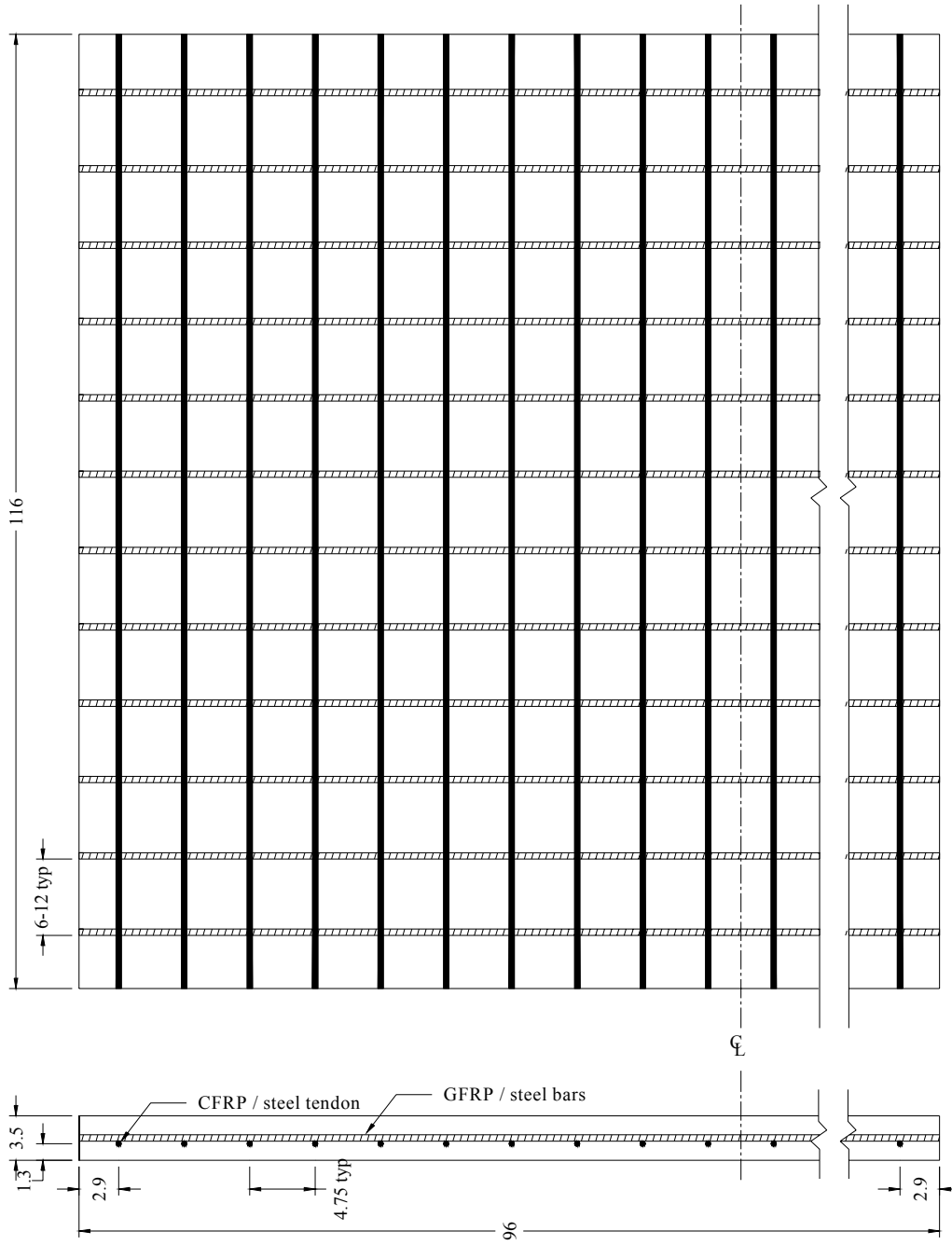
Figure 4.4 - CDOT Panel Cross-Section and Plan View (all values in inches)

4.3.1 Test Setup

Figures 4.5a and 4.5b show the basic setup used to support and load the panels. The simple supports at the ends were constructed using a W14X145 steel beam with a 2-in diameter steel bar welded to the top. In order to keep the panel from local damage at the support, a 0.5-in steel plate was placed along the panel width between the panel and the simple support. Two 110-kip MTS loading actuators were hung from a loading frame centered over the top of the test panel.
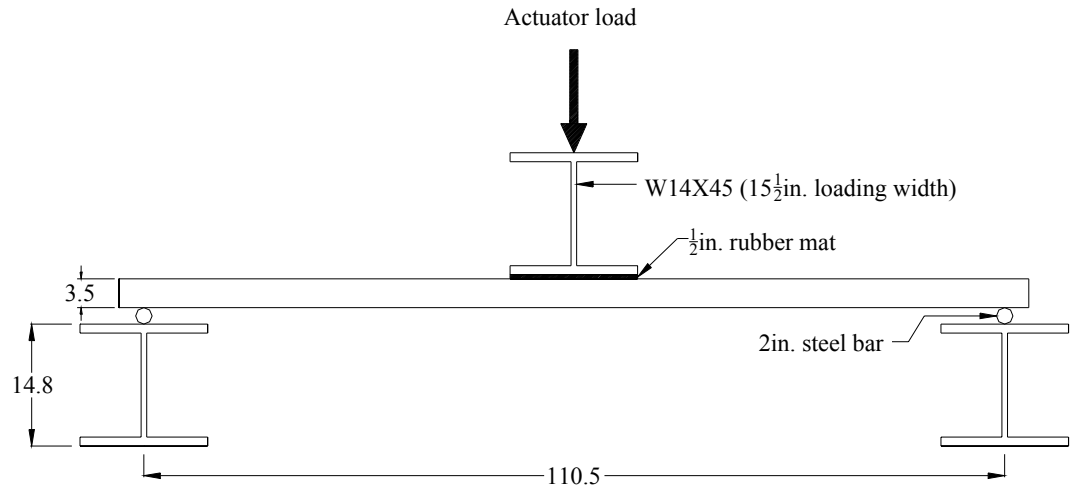
For the panel tests, a W14X145 steel beam was attached to the base of the two actuators as shown in Figures 4.5a and 4.6. On the panel surface, a 0.5-in rubber pad was placed to distribute the load more uniformly. The loading beam was 1.5-in wide and 96-in long to provide a line load.

For the composite slab tests, a 2-in thick, 20-in-by-2-in plate was placed beneath the beam as shown in Figures 4.5b and 4.7. The dimensions of the steel plate were to model the tire contact area recommended by AASHTO.
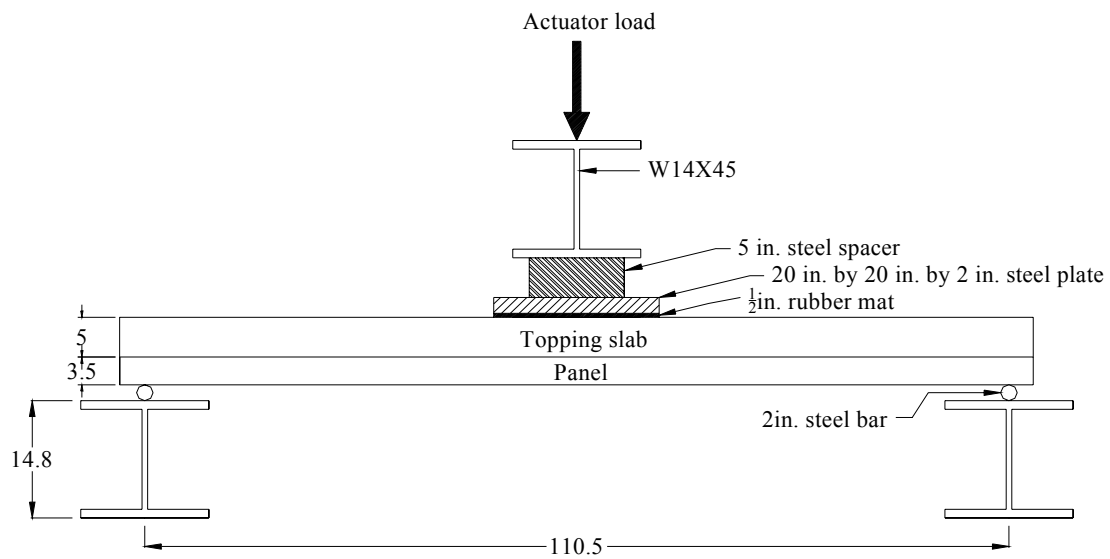
4.3.2 Instrumentation

Linear voltage differential transducers (LVDTs) were used to measure deflection at the mid-span of the panels. The LVDTs were attached to both sides of the panels with glue. The LVDTs measured the distance between the attachment point of the panel and the floor of the laboratory.

Prior to placement of the composite slab, strain gauges were mounted on the reinforcing steel as shown in Figure 4.8. Also displayed in the figure is the elevation view of the reinforcing grid on which the gages were mounted. One layer was placed directly on the panel surface and another layer was raised 3 to 4 in off the panel.

Actuator load

W14X45 ($15\frac{1}{2}$in. loading width)

$\frac{1}{2}$in. rubber mat

3.5

2in. steel bar

14.8

110.5

(a)

Actuator load

W14X45

5 in. steel spacer

20 in. by 20 in. by 2 in. steel plate

$\frac{1}{2}$in. rubber mat

5

Topping slab

3.5

Panel

2in. steel bar

14.8

110.5

(b)

Figure 4.5 - Loading Setups for (a) Panel Tests and (b) Composite Slab Tests
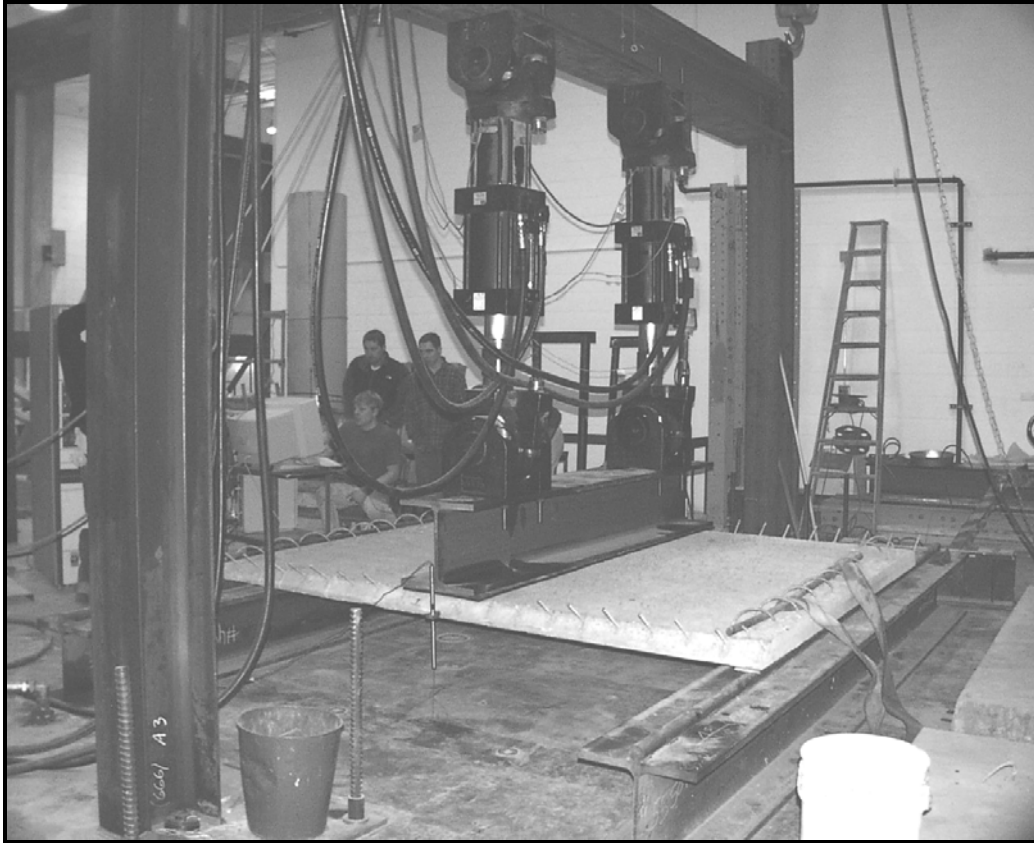(all values in inches)

40

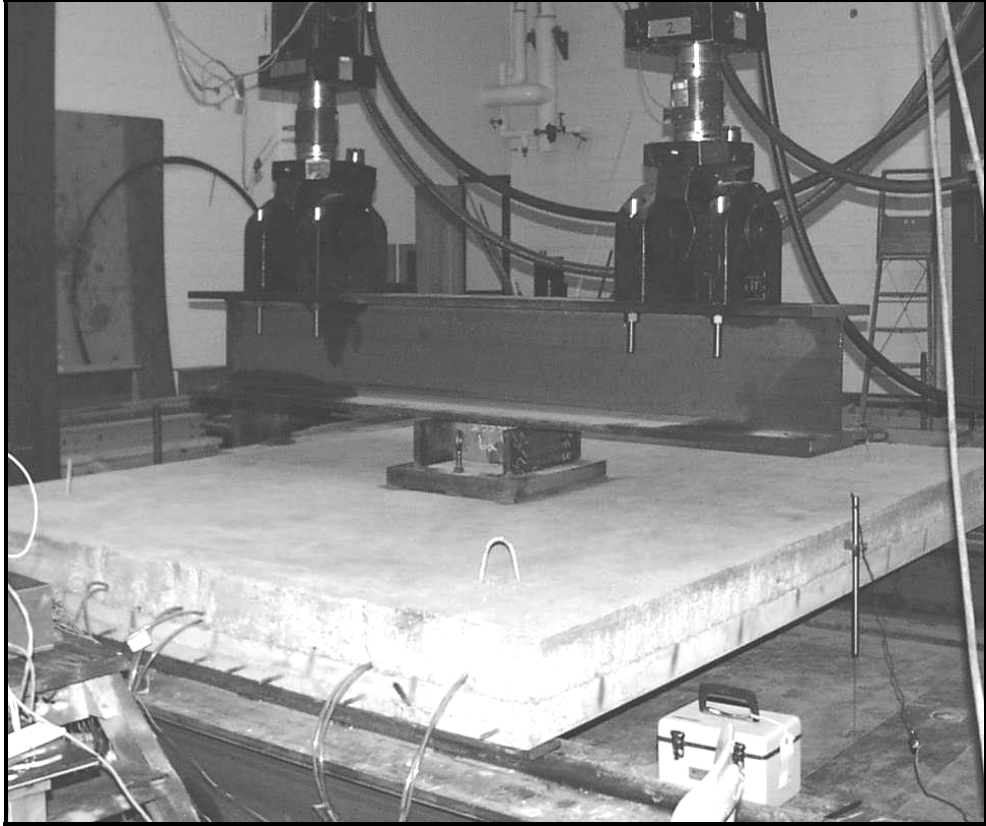Figure 4.6 - Line Load Testing Setup for Panel Tests

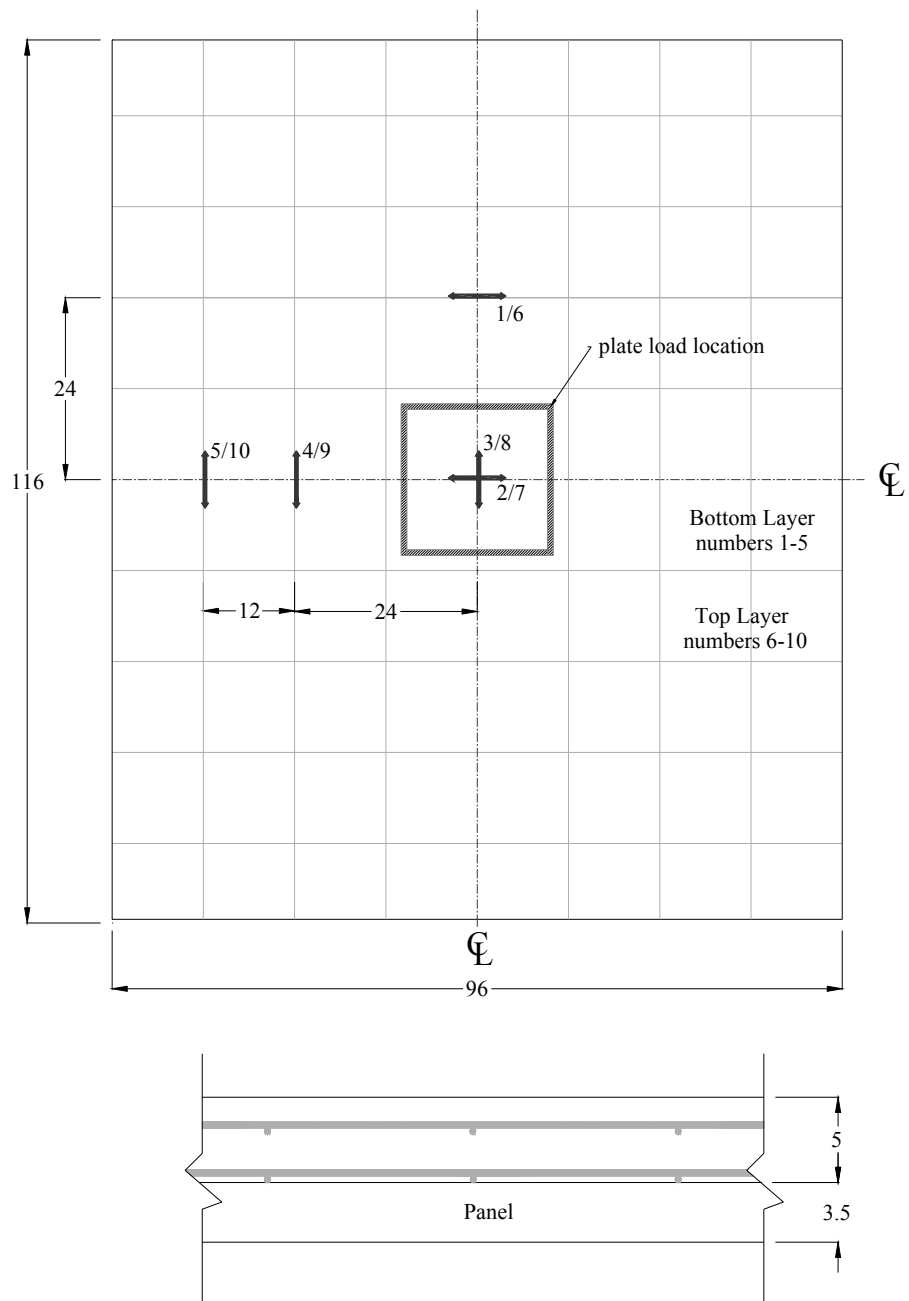Figure 4.7 - Plate Load Testing Setup for Composite Slab Tests

Figure 4.8 - Strain Gage Layout (all values in inches)

4.3.3 Panel Fabrication

The two CFRP prestressed panels were cast six days before the steel prestressed panels were cast, and the CDOT panel was cast several months later. Even though the same high-performance concrete mix design was used for all the panels, the compressive strength of the concrete for the two CFRP prestressed panels was 2,600 psi at prestress release and 3,350 psi at 28 days, compared to 4,500 and 4,900 psi for the steel prestressed panels. Hence, the concrete for the first set was inferior and did not satisfy the design specifications.

4.3.4 Results of Panel Tests

CFRP Prestressed Panel

Immediately upon delivery of the CFRP prestressed panels, small cracks were observed originating at each prestressing tendon as shown in Figure 4.9. Many of the cracks crossed the entire panel as visible on both the top and the bottom surfaces. The cracks are suspected to be caused by the low strength of the concrete (2,600 psi) at stress transfer. When a tendon is prestressed, the diameter reduces due to Poisson's effect. Upon prestress release, the bars expand laterally and induce tensile stresses in the concrete. In this case, the force produced by the tendon expansion might have been too high for the concrete. These cracks were observed only on the CFRP prestressed panels. The steel reinforced panels had adequate concrete strength (4,500 psi) when the prestressing force was released, and no cracks were observed.

The CFRP prestressed panel failed in a typical over-reinforced fashion in which the concrete in the top half of the slab crushed before any tendon failure was observed. However, at some point during the test, the load carrying capacity dropped significantly because of excessive bond slip. This poor bonding can be attributed to the cracks in the vicinity of the tendons as mentioned above. No elastic rebound was observed after release of the load. The load-displacement curve for this test is shown in Figure 4.10.

Compared to the nominal strength calculated with the design parameters, the CFRP panel under-performed considerably. The maximum load was 9.9 kips. This was considerably less

than the expected design load of 18 kips. This can be attributed to the several discrepancies between the design specifications and the actual panel. First, the strength of the concrete on the day of the test was 3,600 psi which is considerably lower than the 4,500 psi strength specified in the design. This has a significant impact on an over-reinforced panel. Second, the depth of the panel was found to be slightly less than the 3.54 in specified in the design. The actual depth was 3.4 in. Finally, the location of the strand was found to be at 1.7 in from the base on the average. This essentially eliminated the eccentricity specified in the design. Based on these three findings, the load carrying capacity of the panel was recomputed and found to be 10.2 kips. This value could be further reduced by the slip of the tendons. In any respect, the calculated value is very close to the test result as shown in Figure 4.10.
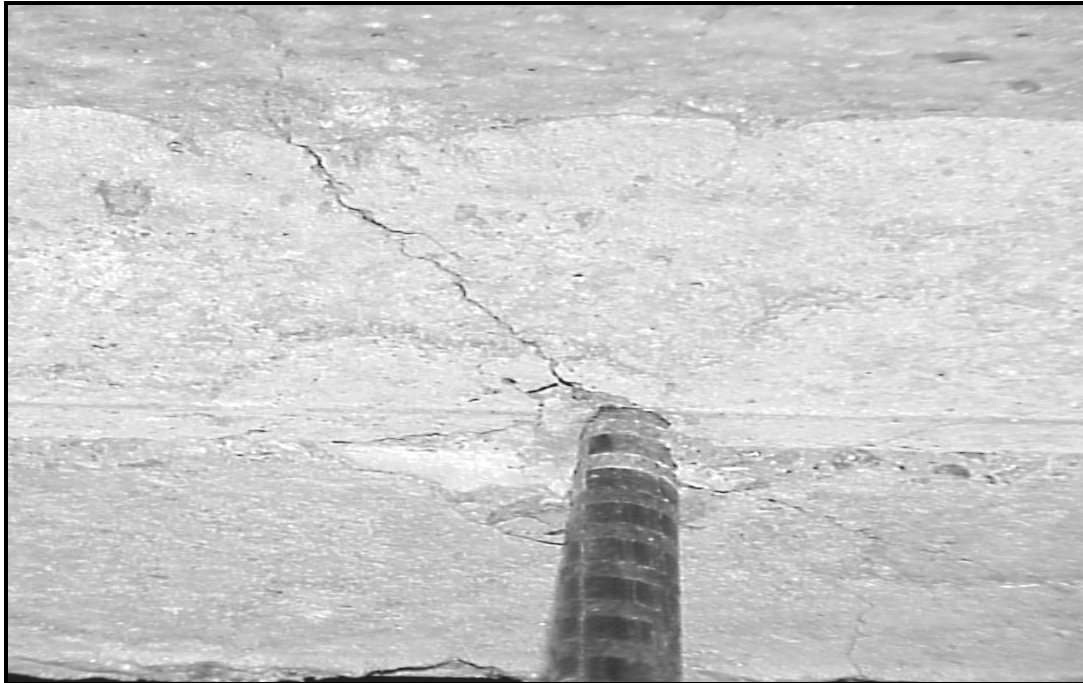

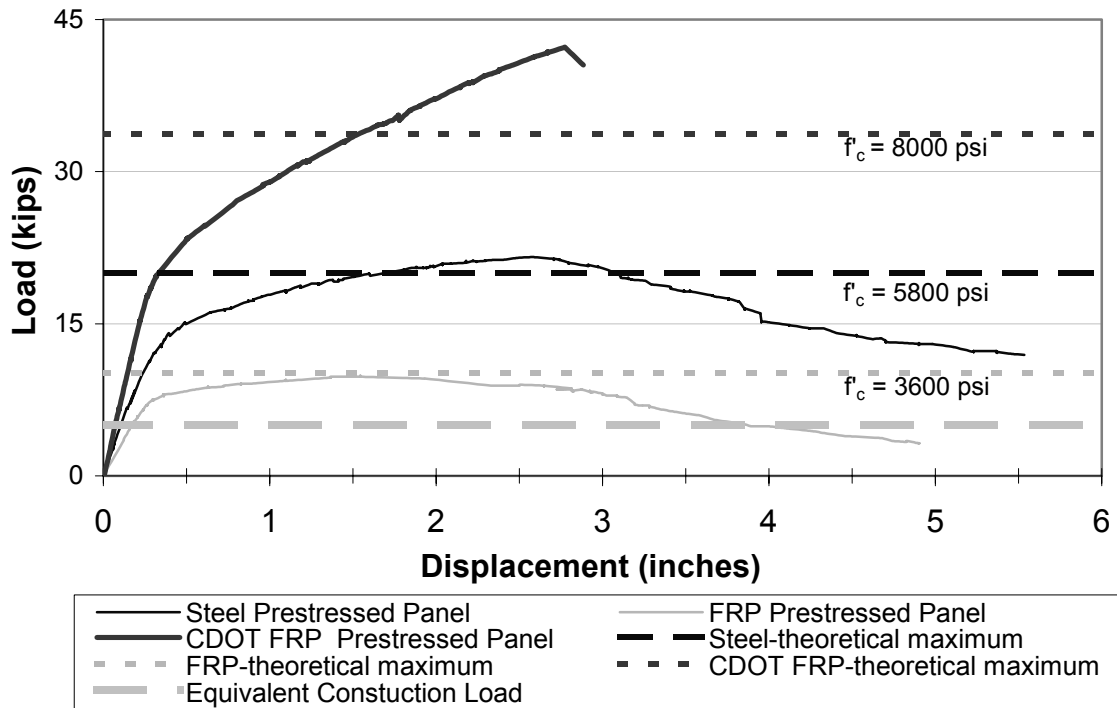Figure 4.9 - Initial Cracking Surrounding the Prestressed CFRP Tendons

Figure 4.10 - Load vs. Displacement Curves for the Three Panels

Steel Prestressed Panel

For the steel prestressed panel, the strength of the concrete on the day of the test was 5,800 psi, which is significantly higher than the design strength of 4,500 psi. This increased the load capacity from 18.4 kips to 20 kips. The location of the steel strand was fairly precise. The panel failed at a maximum load value of 21.6 kips. The failure mode was typical for an over-reinforced member in that the steel strand never ruptured. Upon reaching the maximum stroke of the actuators at 6 in, the load was released. This was followed by an elastic rebound of a few inches. The load-displacement curve is shown in Figure 4.10.

CDOT Panel from the Bridge

The CDOT panel had twenty CFRP tendons, whereas the first two panels had only fourteen tendons. As shown in Figure 4.10, the CDOT panel showed a very high strength and a brittle failure. Upon reaching the maximum load of 42.3 kips, the panel cracked in half with complete rupture of the CFRP tendons and dropped to the floor. The tendon rupture is suspected to be caused by the excessive bending of the tendons under a large panel deflection. Unlike the first CFRP prestressed panel, no signs of tendon-concrete bond failure were observed. Figure 4.11 shows the CDOT panel after failure.

From theoretical calculations, the concrete strength should have significantly exceeded 8,000 psi to reach the panel strength obtained in the test. Unfortunately, the cylinder test result from a field specimen is inconclusive.

Figure 4.10 shows the comparison of the test results to the theoretical load carrying capacities of the panels. In addition, the uniformly distributed construction load specified in the design is converted to an equivalent line load. The equivalent load is 5 kips. It is clear that all panels, including the first CFRP prestressed panel, can adequately meet this construction load requirement.

Steel Prestressed Composite Slab

The load-displacement curve for the composite slab with steel strands is shown in Figure 4.12. The maximum load reached was 96.6 kips. The theoretical nominal load capacity is 76.1 kips considering the entire width of the slab and is 68.8 kips considering the equivalent width of AASHTO. This capacity is computed assuming that there is no slip between the steel strands and the concrete.

The failure of the steel prestressed composite slab was exactly as expected. The slab was under-reinforced meaning that the steel would yield well before the concrete reached crushing levels. As shown in Figure 4.12, the steel reached its plastic regime and retained strength for a

considerable duration. Then, without warning, the strands ruptured and the slab cracked into two halves and fell to the floor. Although development length was the governing criterion for the design giving nominal load capacities of 75.3 kips considering the entire width of the slab and 68.1 kips considering the equivalent width of AASHTO, no bond slip occurred.
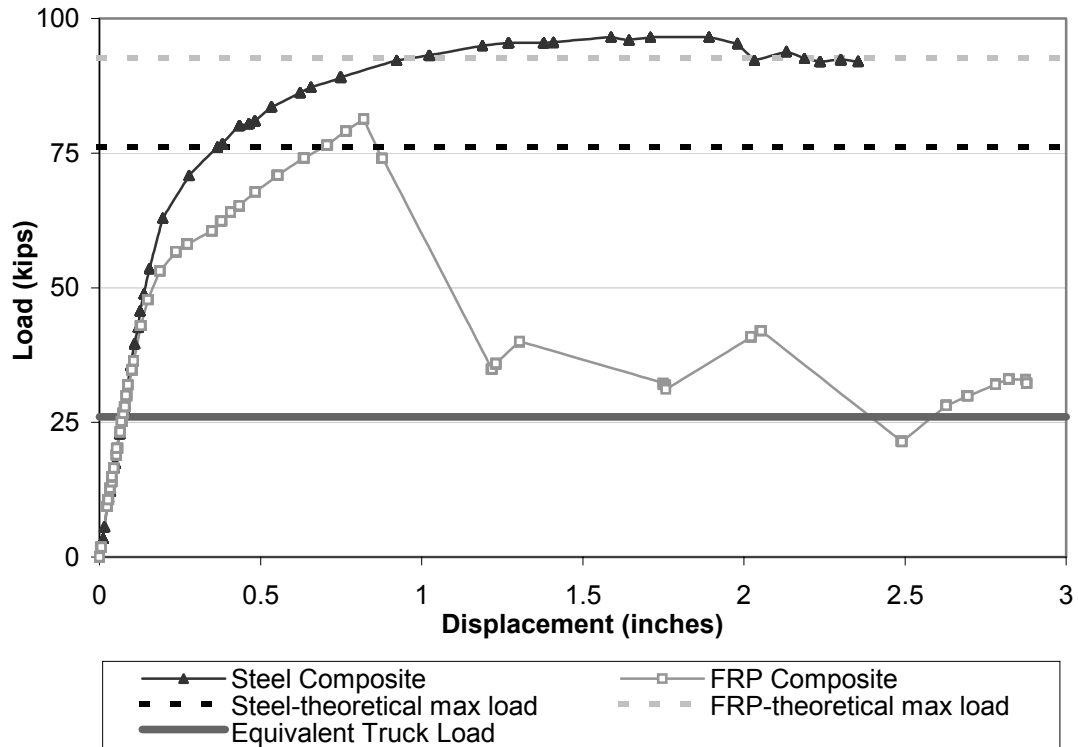

Figure 4.11 -   CDOT Panel Failure

Figure 4.12 - Load vs. Displacement Curves for the Composite Slabs (the theoretical maximum loads were calculated with a full panel width)

CFRP Prestressed Composite Slab

For the CFRP prestressed composite slab, the load-displacement curve is shown in Figure 4.12. The actual maximum load achieved in testing was 81.4 kips. The theoretical nominal load carrying capacity is 98.6 kips considering the entire width of the slab and 89.1 kips considering the equivalent width. This capacity is computed assuming that there is no slip between the CFRP tendons and the concrete. However, if the required development length is considered, the stress that can be developed in the CFRP tendon is significantly reduced because of the limited embedment length available. The theoretical nominal load carrying capacity based on the reduced tendon stress due to debonding is 83 kips considering the entire width of the slab and 75 kips considering the equivalent width.

Numerous observations were made during the testing of the CFRP reinforced composite slab. Once the maximum load was reached, bond slip occurred in a few of the prestressed tendons. This caused a momentary drop in the load resistance of the slab. Then the strength increased again slightly until the next pullout occurred. This process repeated itself. At the end, the panel did not fail completely and was able to support its self-weight. This is shown in Figure 4.12.

4.3.5   Summary of Test Results

Table 4.1 compares the calculated load capacities of the panels and composite slabs with the experimental results and design loads. The *nominal design strength* in the second column was calculated according to the design specifications, while the *theoretical strength* was based on the as-built conditions with the actual concrete strengths on the day of testing. In the last column, the *design loads* are the specified construction load for the case of panels without a topping slab and the wheel load of an HS25-44 truck considering only the impact factor for the case of composite slabs.

For the composite slabs, two numbers are listed in the nominal design strength and the theoretical strength columns. The first number is the equivalent load capacity using the AASHTO equivalent width. The second number is the equivalent load capacity using the full panel width. These capacities are calculated without the consideration of possible bond failure. However, for the FRP prestressed slab, the corresponding strength values considering bond failure are also given (in brackets) in the table.

Furthermore, Table 4.1 compares the ductility of different panels. In this study, ductility is defined as the ratio of deformation of the panel at the peak load to that at the design load. This is obtained from the experimental load-deflection curves. It is interesting to see that the CDOT panel with FRP prestressing tendons had the highest ductility.

For the steel prestressed composite slab, the experimental load achieved in the test far exceeds the theoretical load capacity. For the FRP prestressed composite slab, the experimental load achieved is between the theoretical load capacities with bond slip considering the full and

equivalent widths. It can be concluded that in this case, the slip of the tendons was the governing factor for failure.

Table 4.1 - Panel Ductility and Comparison of Design and Theoretical Strengths to Test Results

Panel Type	Actual Concrete Strength On Test Day *psi*	Nominal Design Strength *kips*	Theoretical Strength *kips*	Experimental Values *kips*	Ductility	Design Load *kips*
CDOT Panel	NA	NA	33.7	42.3	33	
Steel Prestr. Panel	5,754	18.4	20.0	21.6	21	5
FRP Prestr. Panel	3,661	18.0	10.2	9.9	8	
Steel Prestr. Comp. Slab*	*Topping Slab* 3,553	71.1 / 78.6	68.8 / 76.1	96.6	19	26
FRP Prestr. Comp. Slab*	*Topping Slab* 3,553	93.7 / 103.6	89.1 / 98.6 [75/83]	81.4	8	

* The two numbers listed represent the equivalent load capacity using the AASHTO equivalent width and the full panel width, respectively.

For all five tests performed, the strengths satisfy the design loads with a large factor of safety.   Furthermore, the results seem to indicate that the Equivalent Width Strip method of AASHTO is conservative.

5. Evaluation of a Model Deck with Fatigue Load Cycles

5.1 Introduction

The bridge deck at the I-225/Parker Road interchange has post-tensioned reinforced concrete box girders. On top of the girders, 3-1/5-in-thick precast concrete panels were placed as stay-in-place forms and a 5-in-thick cast-in-place topping slab was poured to result in an 8-1/2-in composite slab. Some of the panels were pretensioned with CFRP bars as one objective of the IBRC project. To evaluate the strength and long-term performance of the composite slab that has CFRP prestressed panels, a model bridge deck was built and tested under static and fatigue loads. However, unlike the actual deck that has post-tensioned concrete box girders, the test deck had the slab support on three steel girders. The composite slab in the deck was made of 3-in-thick precast panels and a 3-in topping, as shown in Figure 5.1. The 6-in composite slab approximately represented a 2/3-scale model of the actual bridge slab. Since a minimum thickness of 3 in was required for the precast panels from the construction standpoint, an exact scaling was not possible here.
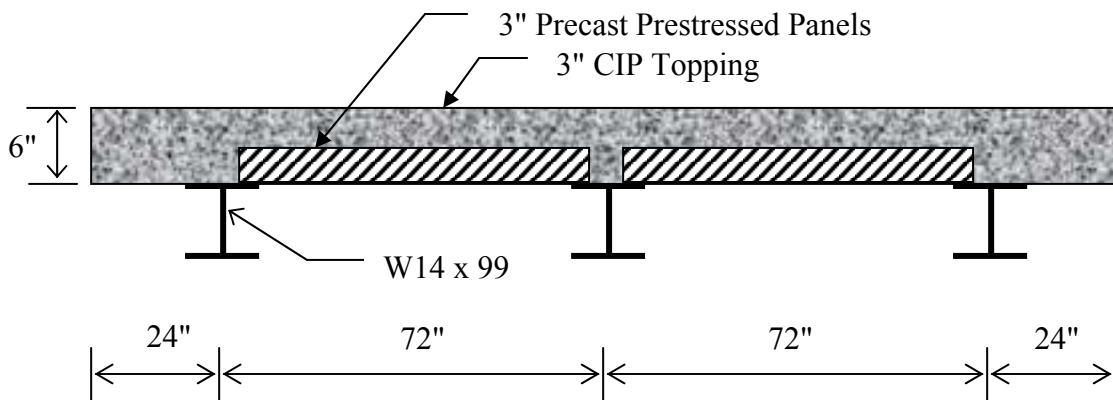

Figure 5.1 – Cross-Section of Precast Prestressed Panel Deck with Cast-in-Place Topping

In addition to the aforementioned objective, the test deck was designed and constructed for the following investigations: (a) evaluating and comparing the performance of bridge decks designed with the empirical and conventional methods of AASHTO (AASHTO 1998), and a new

limit-state design approach proposed in this study; (b) studying the applicability of the AASHTO empirical method to cast-in-place topping slabs in bridge decks that have precast panels as stay-in-place forms; and (c) examining the influence of lap splices between precast panels on deck cracking.

To fulfill the above goals, a segment of the test deck had full-depth cast-in-place concrete, and the remainder had a composite section with precast prestressed panels as stay-in-place forms and a cast-in-place reinforced concrete topping. Half of the precast panels contained steel reinforcement to serve as control panels and the other half contained FRP reinforcement. Furthermore, the deck was divided into segments that were designed with the limit-state method proposed in this study (Shing, Borlin, and Marzahn 2003), the AAHTO empirical method, and the AASHTO conventional method, respectively. The deck span was 30 feet with a 2-ft overhang at each end. It was designed to carry its self-weight and a scaled-down HS-25 design truck that had a wheel load of 8.89 kips.

5.2 Deign of Test Deck

The deck consisted of four segments, each having a different design. Figure 5.2 shows a plan view of the deck and the design methodology used for each segment of the deck. Segment A had a composite slab with a topping slab designed with the AASHTO empirical method. It must be mentioned that the use of the empirical method for the topping slab with precast panels as stay-in-place forms is currently not permitted by AASHTO. Its inclusion in this study was to evaluate its potential applicability. Segment D had a full-depth cast-in-place slab that was deigned with the empirical method. Segment B had a composite slab designed with the AASHTO conventional method, and Segment C had a composite slab designed with a limit-state approach (Shing, Borlin, and Marzahn 2003). The simple supports were located right at the edges of Segments A and D with a 24-in overhang at each end.

The panels on the north side were control panels that had 3/8-in-diameter seven-wire steel strands for prestressing and No. 3 steel bars as mild reinforcement, while those on the south side had 8-mm (0.315 in) Leadline CFRP bars for prestressing and No. 4 GFRP bars from Marshall

Industries as temperature/shrinkage reinforcement. As shown in Figure 5.2, only three of the panel-to-panel joints had full lap splices. The remaining joints did not have any splicing bars. For the joints between the precast panels and full-depth cast-in-place slab, splicing bars were only provided by the precast panels.

Figures 5.3 and 5.4 show plan views of the top and bottom reinforcement. Figures 5.5 and 5.6 show transverse section views of the full-depth cast-in-place portion of the deck and the precast prestressed panel portion of the deck. Finally, Figure 5.7 shows a plan view and a cross-sectional view of the precast prestressed panels with splicing bars. The splicing bars shown are frequently used for this type of construction by the Colorado Department of Transportation.

It should be pointed out that the precast panels were all designed with an allowable stress approach regardless of the design method used for the composite slab.

As shown in Figure 5.3, the empirical method resulted in a significant reduction in the top reinforcement, whereas the proposed method led to a reinforcement level that was slightly higher than that required by the empirical method. For the full-depth cast-in-place segment designed with the empirical method (Segment D), the total reinforcement was significantly less than what would have resulted if it was designed with the conventional method.

The details of the design process can be found in the report by Shing, Borlin, and Marzahn (2003).
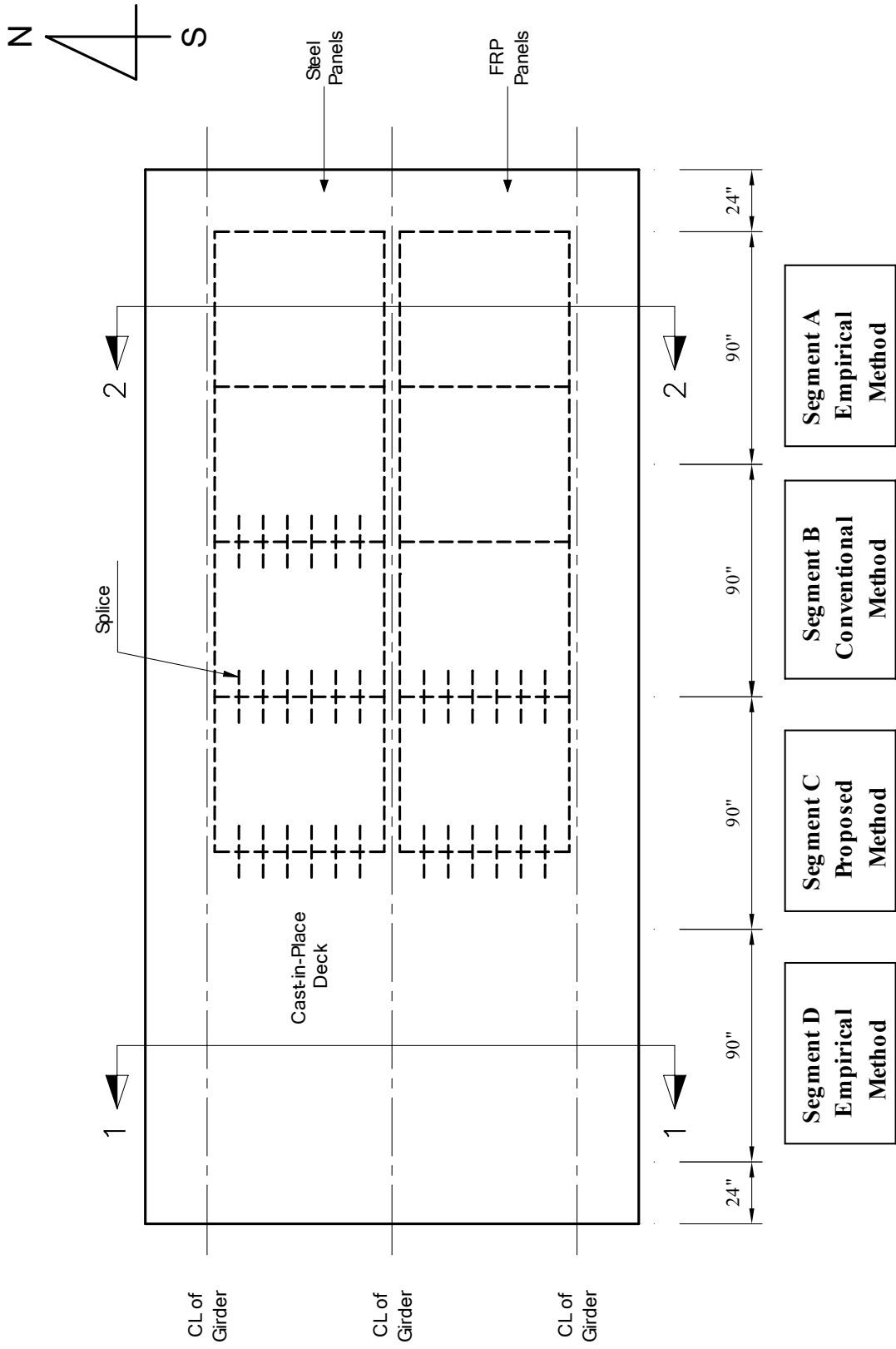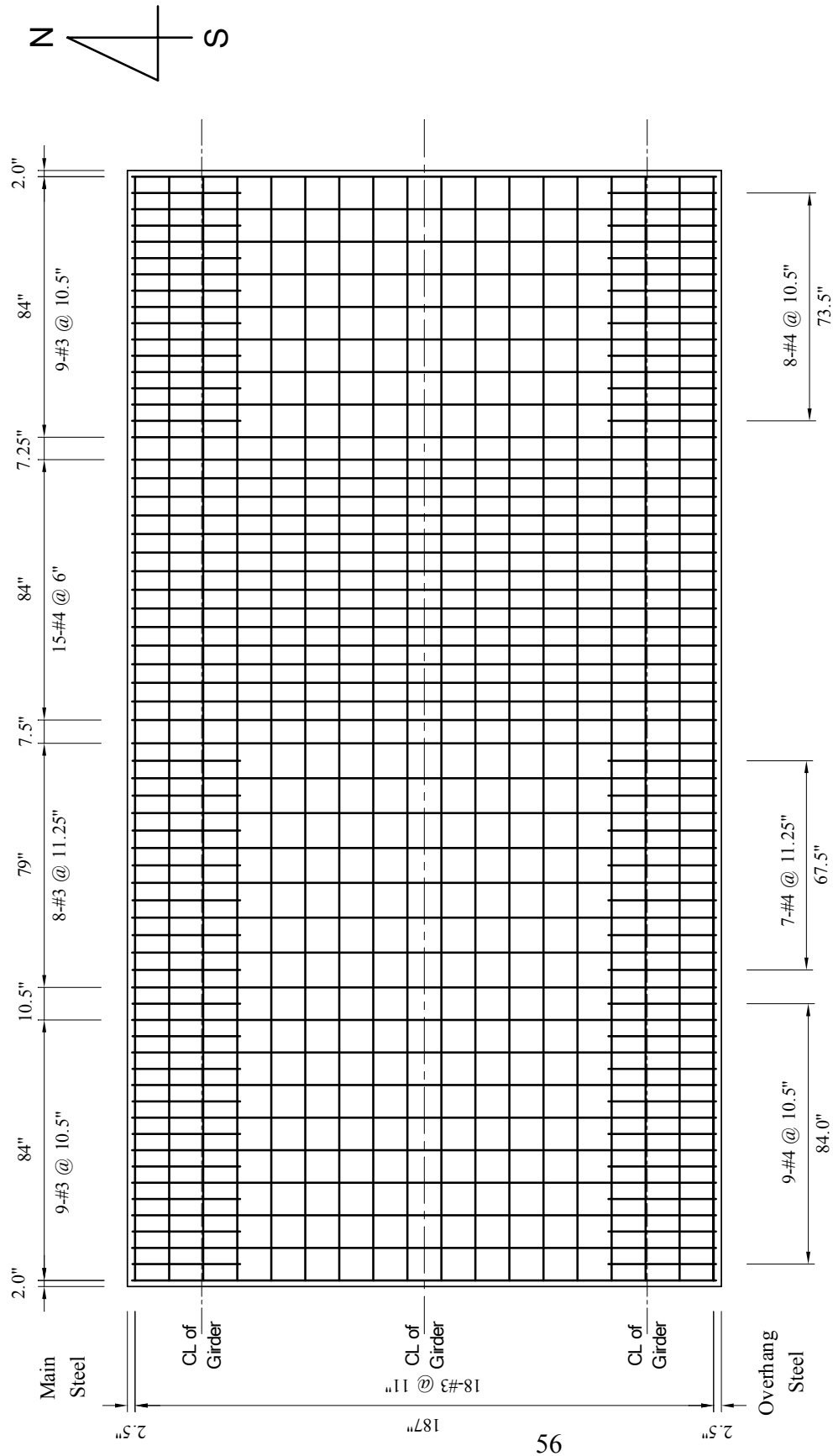
Figure 5.2 – Plan View of Deck

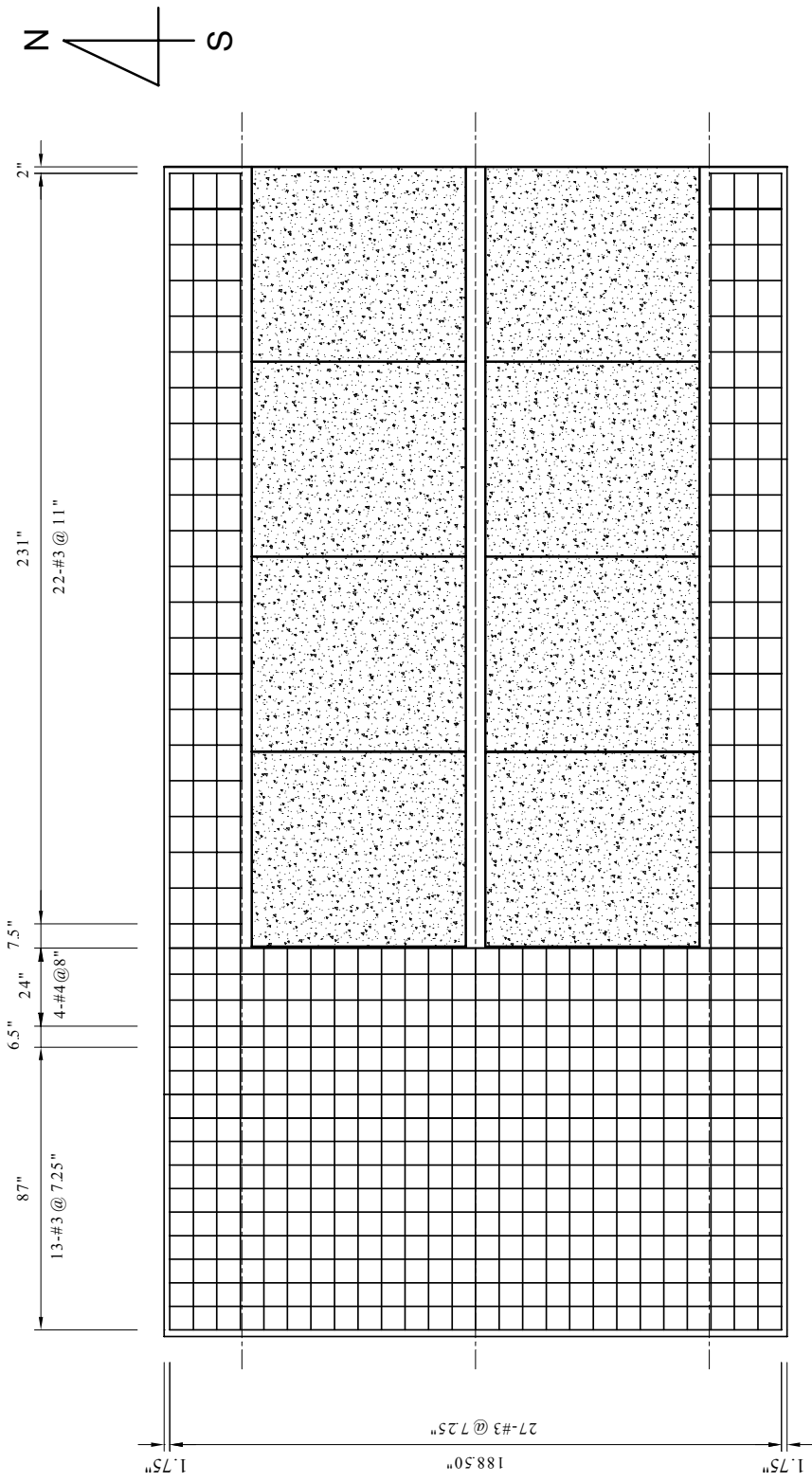Figure 5.3 – Plan View of Top Reinforcement (Support to Support only)

Figure 5.4 – Plan View of Bottom Reinforcement (Support to Support Only)

6"

24"

72"

72"

24"

1.5"

1.5"

#3 bars @ 11" C.C.

#3 bars @ 7.25" C.C.

7/8" Shear Connectors (6" long)

W14x99

1" haunch typ.
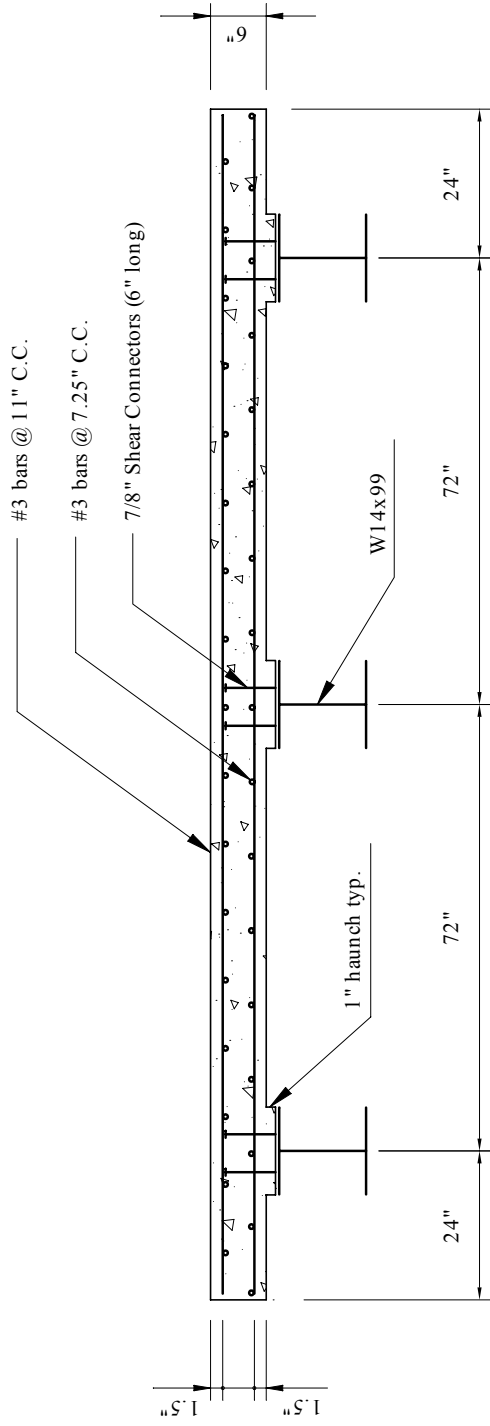
SECTION 1-1

Figure 5.5 – Cross-Section of Full-Depth Cast-in-Place Deck

58

SECTION 2-2

Cast-in-Place Topping

3" Precast Prestressed Panel

#3 bars @ 11" C.C.

7/8" Shear Connectors (6" long)

#3 bars @ 7.25" C.C

1" haunch typ.

W14x99

6"

24"

72"

72"

24"

1.5"

1.5"
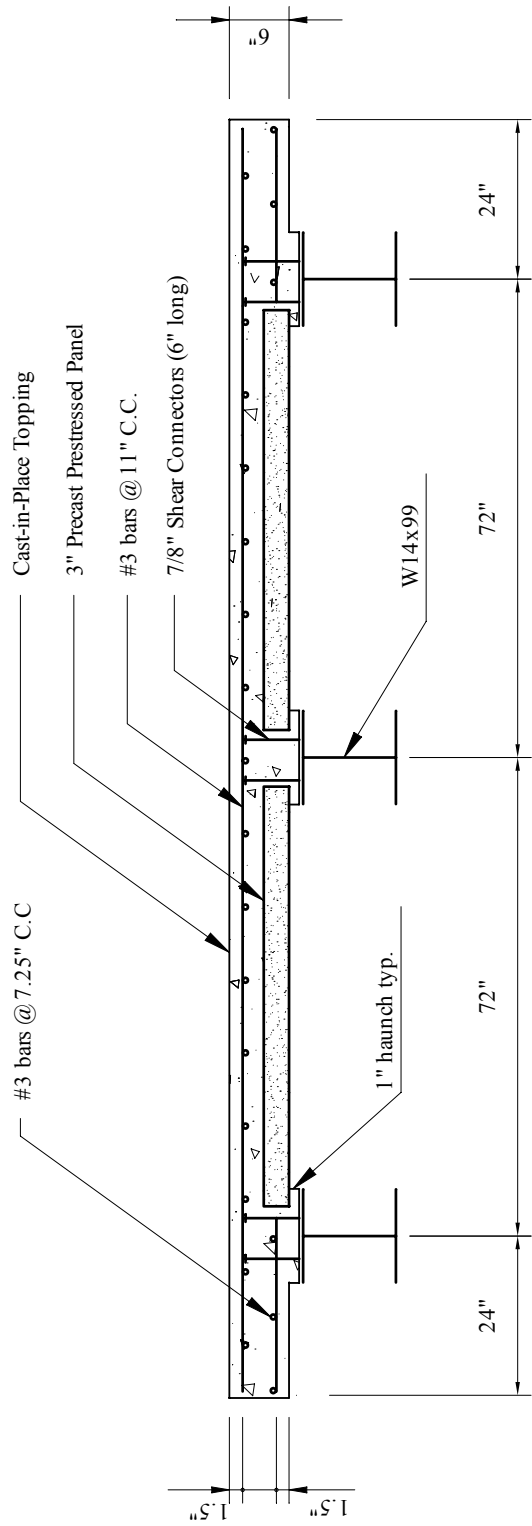
Figure 5.6 – Cross-Section of Precast Panel Deck
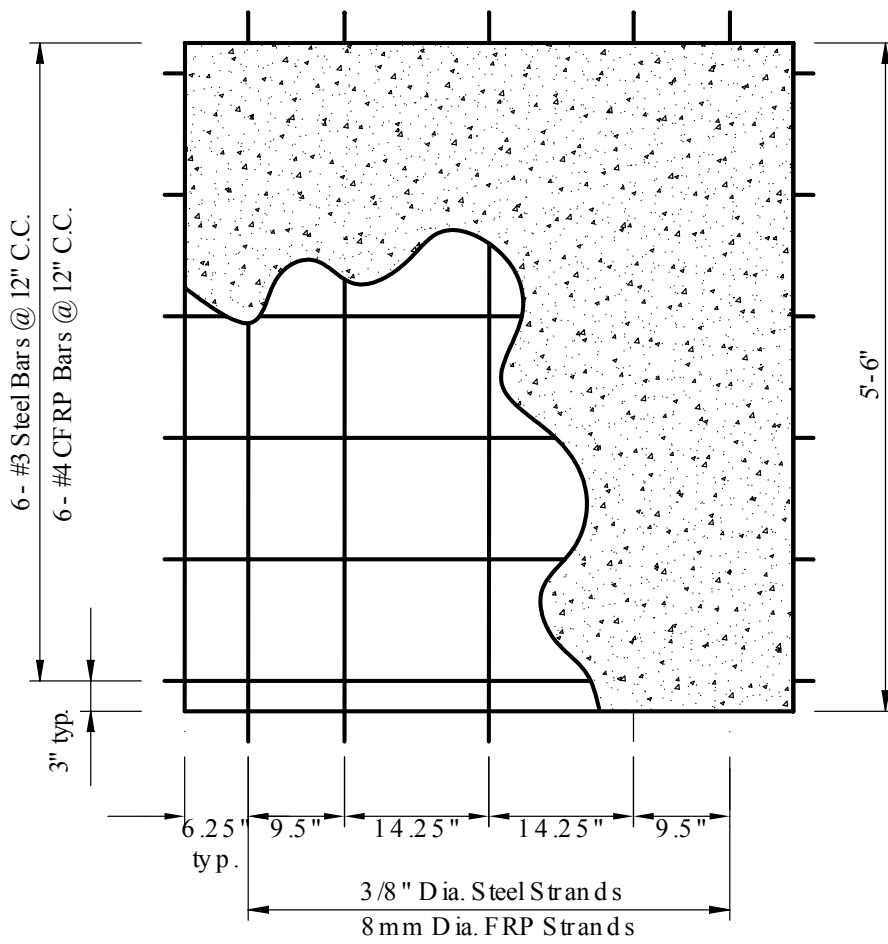
Plan View

Section View

Figure 5.7 – Precast Panel Design

5.3 Test Setup

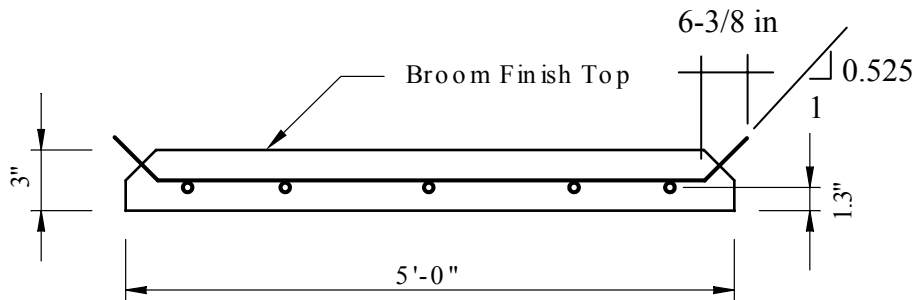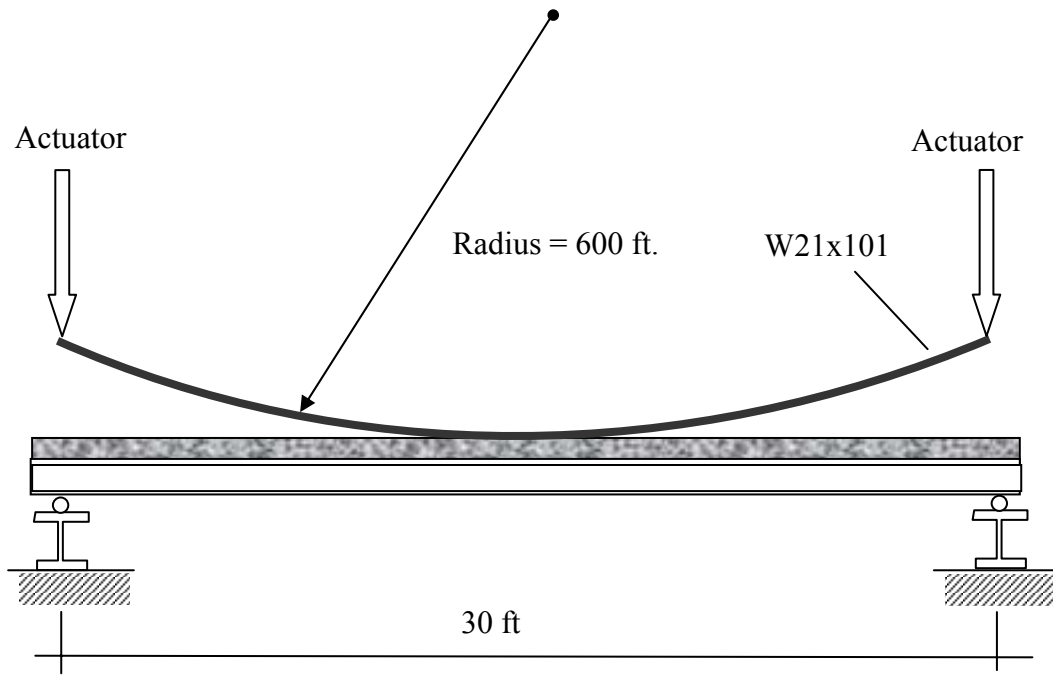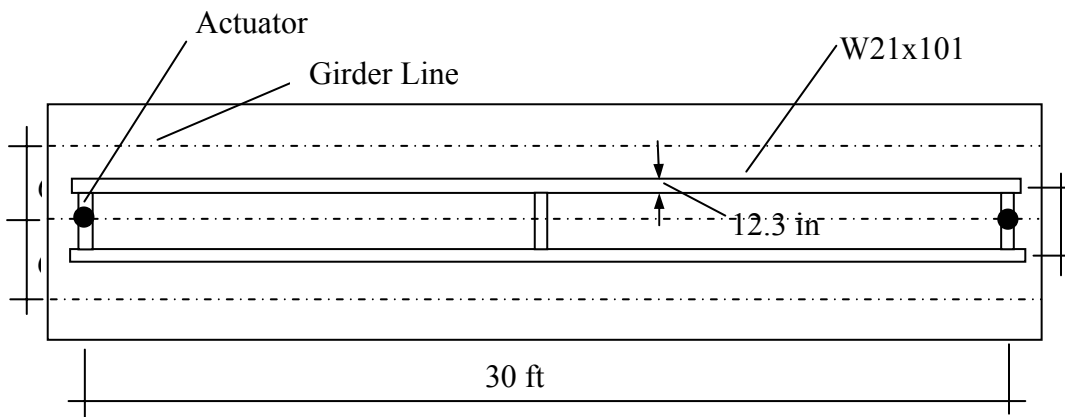The test setup was designed for both static and fatigue tests. To simulate a moving truck load, the fatigue test was conducted with two rocking curve beams as shown in Figure 5.8. The beams were made of W21x101 steel sections, and were bent into a circular arc with a radius of 600 ft. They were spaced at a center-to-center distance of 5 ft. The flange width of each beam was 12.3 in. Half-inch thick rubber pads were placed between the beams and the concrete surface of the deck to assure a more uniform load transfer.

The dimensions of the curve beams were selected based on the footprint of an HS-25 truck tire and the 2/3-scale of the test deck. According to the AASHTO LRFD Specifications (AASHTO 1998), the tire area of an HS-25 truck is 20-in long and 18.6-in wide. This leads to a scaled tire area of 13.3 in x 12.4 in. For this reason, a 12.3-in-wide steel beam section was chosen. The radius of curvature of the beams was determined by the total stroke of the actuators, which was 10 in. The contact length between a curve beam and the surface of the deck was estimated with the elastic contact theory to be close to the scaled length of a tire. Since it depends on the beam curvature, bending stiffness of the beam, and the stiffness of the rubber pads, it is difficult to estimate the contact length in an accurate manner. The distance of the wheels in a single axle of an HS-25 truck is 6 ft. For a 2/3-scale model, this leads to a wheel spacing of 4 ft. However, a 5-ft spacing was chosen to impose a more severe loading condition on the deck. A picture of the test setup is shown in Figure 5.9.

Static load tests were conducted before and after the fatigue load test to measure any change in the load resistance properties of the deck caused by fatigue load cycles, and to examine the final ultimate load resistance of the deck. As shown in Figure 5.10, a pair of static loads were applied to each of the four segments of the deck at a time by attaching the two actuators to a load frame that was orthogonal to the one used for the fatigue test, as shown in Figure 5.9. The loads were applied with 2-in-thick, 13-in-x-13-in steel plates, and there was a ½-inch-thick rubber pad between the plates and the deck to assure a more uniform load application.

Actuator   Actuator

Radius = 600 ft.   W21x101

30 ft

(a) Elevation View

Actuator   W21x101

Girder Line

12.3 in

30 ft

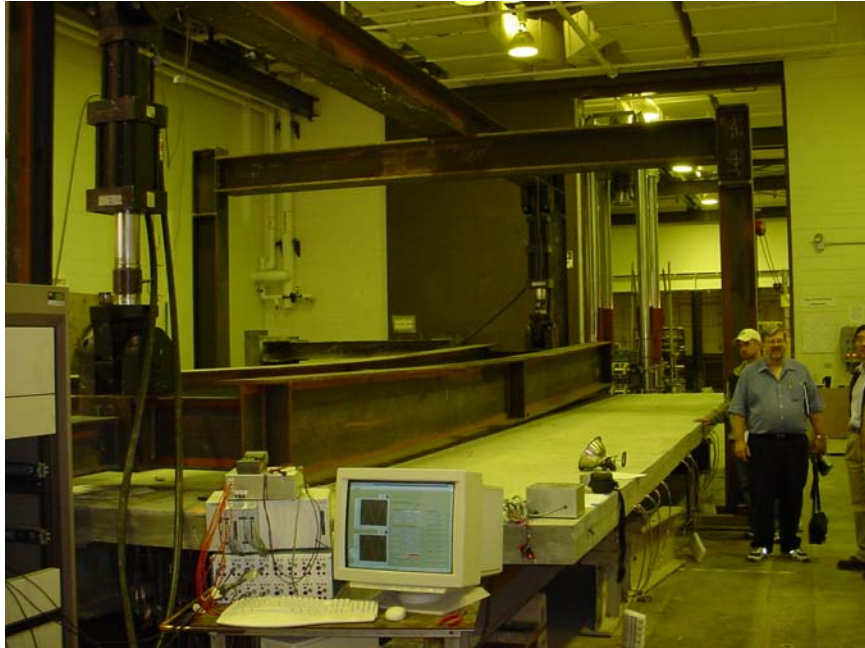(b) Plan View

Figure 5.8 – Setup for Fatigue Test

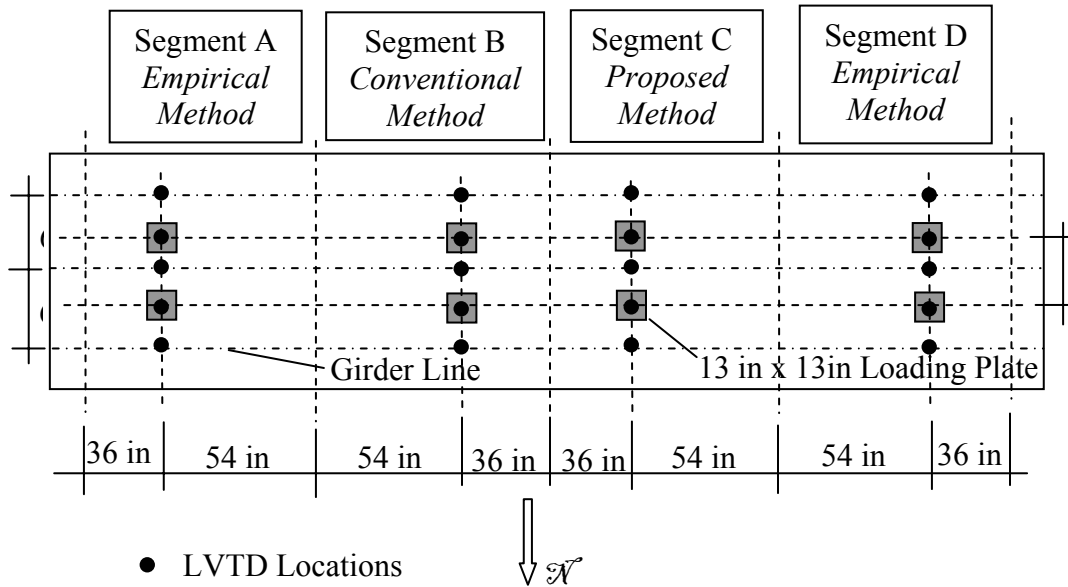Figure 5.9 – Picture of Fatigue Test Setup

Figure 5.10 – Loading and LVDT Positions for Static Load Tests

5.4   Test Procedure and Instrumentation

5.4.1   Fatigue Test

In the fatigue test, the curve beams were rocked back and forth with a pair of actuators as shown in Figure 5.9. Each of the actuators had a load capacity of 110 kips. The actuators were under load control and driven by a sine wave function with a frequency of about 0.14 Hz. They were synchronized with a 180-degree phase angle. This resulted in a moving load that had a linear velocity of about 8.6 ft/sec. The actuators were controlled by electronic servo-hydraulic controllers, one of which had a function generator to generate a sine wave and a load cycle counter.

The total weight of the curve-beam assembly was measured to be around 7 kips. It was taken into account in determining the actuator loads. Two levels of load amplitudes were applied in the fatigue test that had a total of 160,000 load cycles or 320,000 load passes. For the first 62,000 cycles, the load in each actuator varied from 40.5 kips in compression to 2.5 kips in tension. With the self-weight of the curve beams, this resulted in a total compressive load of 22.5 kips exerted by each beam. The travel span of the load was calculated to be 28.7 ft. For the 2/3-scale deck, the scaling factor for load is 4/9. Therefore, including the impact factor, the wheel load of a scaled HS-25 truck was 11 kips. The fatigue load amplitude was, thereby, two times the design truck load.

For the remaining 98,000 cycles, the amplitude of the load in each actuator varied from 63.3 kips in compression to 2.5 kips in tension. This resulted in a total compressive load of 34 kips exerted by each beam, which was 3 times the design truck load. The travel span of the load was calculated to be 29.1 ft.

5.4.2   Static Tests

Before and after the fatigue test, static load tests were conducted with a pair of actuators on each segment of the deck as shown in Figure 5.10. Testing each segment with a pair of static loads required moving the load frame from one location to the other. The exact positions of the

loads along the deck, as shown in Figure 5.10, were determined by the locations of the anchoring holes in the laboratory floor that were used to secure the load frame.

Before the fatigue test began, each segment of the deck was loaded simultaneously with two actuators up to a load of 22 kips in each actuator. Strain and deflection readings were taken. After the fatigue test was completed, these tests were repeated with a maximum load of 30 kips in each actuator. After this, the deck was loaded with one actuator at a time, up to the maximum capacity of the actuator or the failure of the deck, to examine the ultimate load resistance of the concrete slab.

5.4.3   Instrumentation

Strain gages and LVDT's (Linear Variable Differential Transformers) were installed to measure the strains and deflections of the deck at various locations. As shown in Figures 5.10 and 5.11, a group of sensors was installed in each segment of the deck. Figure 5.10 shows the positions of the LVDT's, which were all located along the same line as the applied static loads. Two of the LVDT's were directly under the applied loads and three were under the girders. The LDVT's were moved from one segment of the deck to another as the loading positions changed.

Figures 5.11 and 5.12 show the exact locations and numbering of the strain gages. The strain gages in the cast-in-place portion of the deck were glued onto rebars as shown by Sections A-A and C-C in Figure 5.12. Two bars were installed at each location to obtain two strain readings along the depth of the slab. In regions where there were precast panels, only one bar could be used at each location as shown by Section B-B in Figure 5.12. To have two strain readings at each location in this region, a surface gage was attached to the bottom of the slab. Figure 5.13 shows the attachment of strain gages to rebars, which were later embedded in concrete at the designated locations. Each bar had two strain gages along its circumference, and was oriented in such a way that one gage was at the top and the other at the bottom to average out the localized bending effect of the bar.
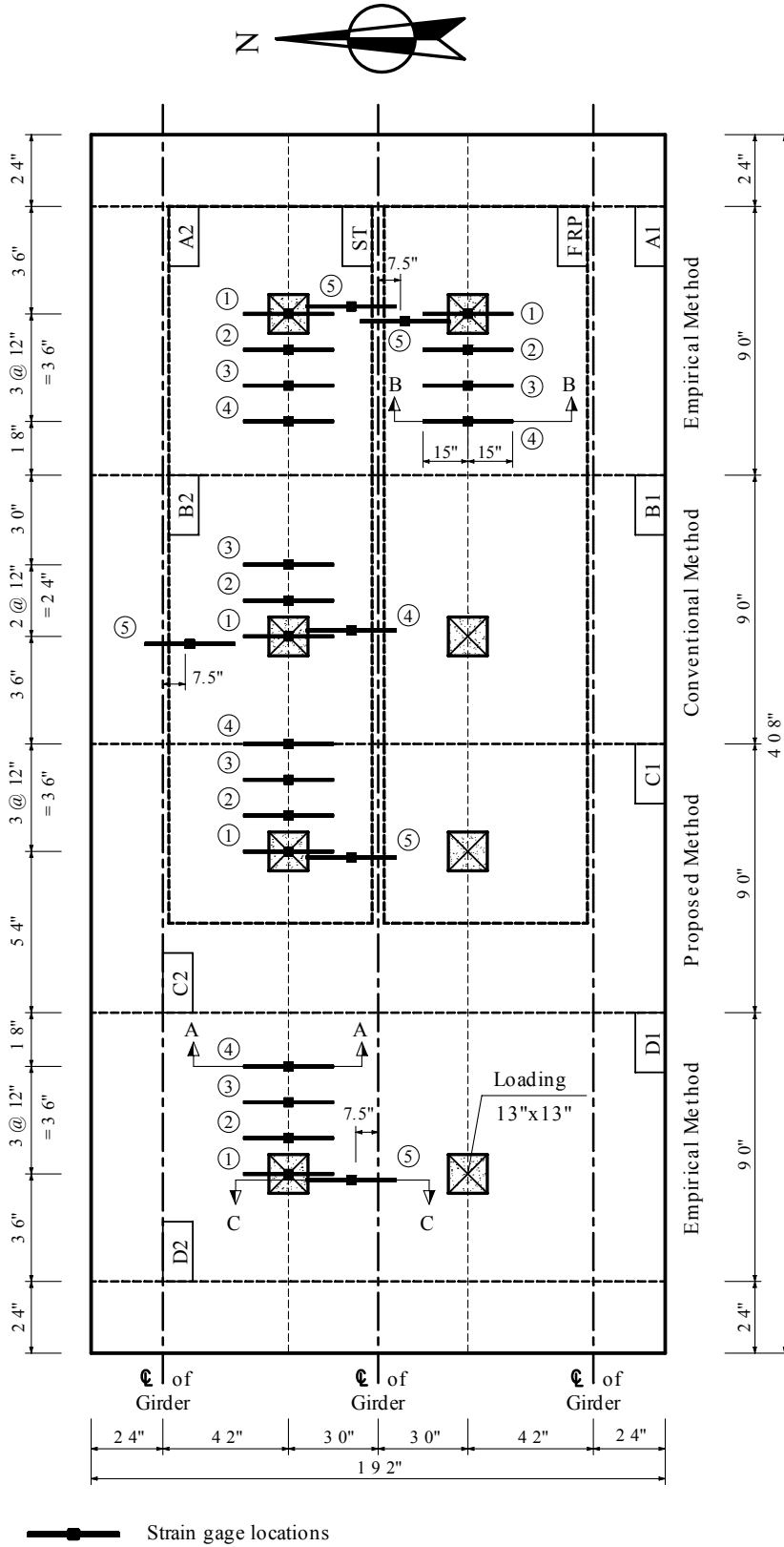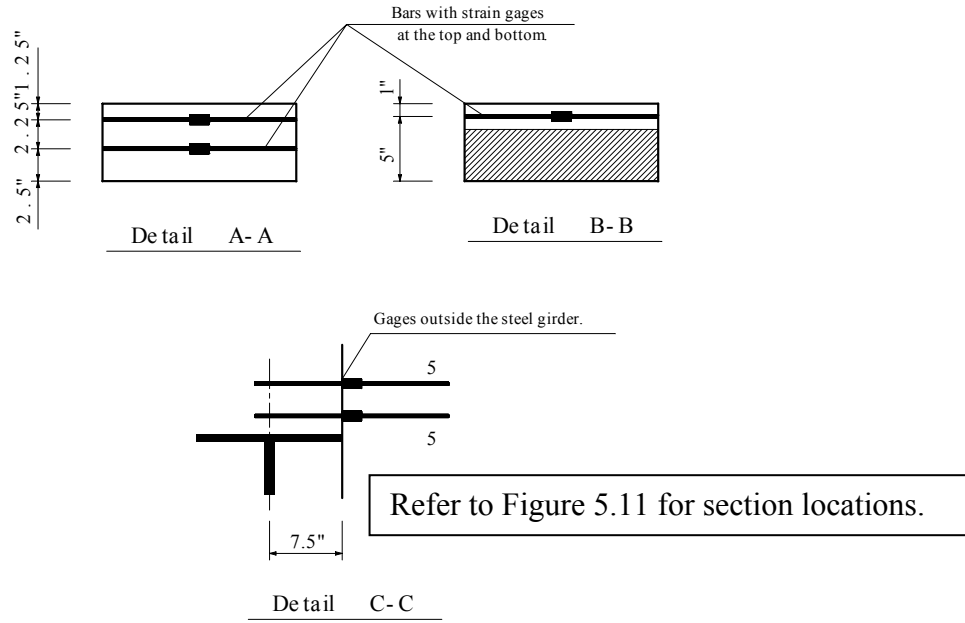
Figure 5.11 – Strain Gage Scheme

66

Figure 5.12 – Strain Gauge Locations along the Depth of the Slab

Figure 5.13 –Bars with Strain Gages

All data were collected by a 16-channel data-acquisition system. The two gages on each bar were wired in such a way that only the averaged readings were recorded by a data-acquisition channel. During the static load tests, only the LVDT's and gages in the segment that was loaded were connected to the data-acquisition system. Because of the limited number of data channels, each static test was conducted two times. The first was to collect load-deflection information, and the second to collect strain readings.

5.5   Test Results

Under fatigue load cycles, Segments A, B, and C of the bridge deck, which had precast panels, demonstrated a better performance than segment D, which was cast in place. The prestressing force in the precast panels delayed/prevented the cracking of the deck and, therefore, improved its endurance under fatigue load cycles.

After 160,000 fatigue load cycles (or 320,000 load passes), the deck was still able to develop a significant arching mechanism that led to a very high load resistance in the final static load tests. Segment D had punching shear failures at a load of about 102 kips, which is slightly under the theoretical prediction of 111 kips. The punching shear capacities of segments A, B, and C were higher than the prediction. This indicates the contribution of the prestressing force, which is ignored in the theoretical prediction, to the punching shear strength. In summary, after 160,000 of fatigue load cycles, the strength of the deck was still at least 10 times the design truck load.

Segments A, B, and C showed comparable performances. Segments A and B, whose top reinforcement was selected according to the empirical method and the conventional method of AASHTO, respectively, had no bottom cracks, while segment C, whose top steel was selected with the proposed limit-state method, had bottom cracks developed in the positive moment regions. These cracks were, however, extensions of the cracks developed in segment D.

There was no visible difference in the performances of the south and north sides of the deck, which had CFRP prestressed panels and steel prestressed panels, respectively.

No reflection cracks were observed on the top surface of the deck right above the joints between the precast panels. The absence of lap splices at some panel joints did not seem to promote reflection cracks.

In general, the precast panel portion of the deck performed well under fatigue load cycles. No delamination between the panels and the cast-in-place topping slab was observed.

5.6   Conclusions

From the load resistance standpoint, CFRP bars seem to be a viable alternative to steel tendons for precast panel construction. The portion of the bridge deck that had CFRP prestressed panels demonstrated the same performance as that with steel prestressed panels. In the example considered in this report, the limit-state design method developed in this project resulted in a reinforcement quantity that is comparable to the empirical method of AASHTO. The former is, however, a more rational approach based on a rigorous analytical procedure.

The test results show that the segments of the deck that had the topping slabs designed with the empirical method and the limit-state method exhibited the same performance as that designed with the conventional method, even though the latter required 70% more reinforcement in the topping slab. Furthermore, with the use of the empirical method, the segment (segment A) of the deck that had precast panels performed better than the full-depth cast-in-place segment (segment D) due to the enhanced strength and crack resistance introduced by the prestressed panels.

The use of the AASHTO empirical method for the design of the topping slab of a precast panel deck does not seem to jeopardize the deck performance under fatigue load cycles. The empirical method can lead to a significant reduction of the top reinforcement in such a deck. It will not only save construction costs, but will also prolong the life span of a bridge deck that has steel reinforcement by reducing corrosion problems. Therefore, it is recommended that the empirical method be allowed for the design of the topping slab for precast panel decks.

The limit-state design method proposed in this project will result in a reinforcement quantity

that is comparable to the empirical method of AASHTO. The former is, however, a more rational approach based on a rigorous analytical procedure. With more calibration and evaluation, this method can be adopted in the design practice.

6. Conclusions

6.1 Optimal Concrete Mix Designs

Considering the overall performance of the concrete mixes tested, a desired range of values for the concrete mix design parameters can be determined. The desired range for cement content is from 465 to 485 lb/yd^3; water/cementitious ratio from 0.37 to 0.41; and Class F fly ash from 20% to 25%. It is found in this study that Class F fly ash results in better durability performance than Class C fly ash. Recommended curing time is seven days.

Two mix designs are recommended for use in the summer and in the winter, respectively. In the summer season, Mix II4-4 is preferable. It has a low cement content of 465 lb/yd^3 and a high fly ash content of 25% of cement by weight. The water/cementitious material ratio can be slightly increased if necessary to improve workability. In the winter season, Mix II8 is preferable. It has higher cement content and lower fly ash content than Mix II4-4. In Mix II8, gravel content could be increased to 1780 lb/yd^3 and w/c could be slightly reduced. In both mixes, Class F fly ash should be used.

For the thin overlay concrete, Mix SFSP-F, II4-4, or II8 can be selected. If Mix II4-4 or II8 is used for thin overlays, smaller aggregate should be used in the mix.

Compared with Class DT, the new mixes developed in this study are more crack resistant and have higher fly ash content with the cement content reduced from above 600 lb/yd^3 to below 500 lb/yd^3. For the new mixes, the chloride permeability is reduced from about 6000 Coulomb (at 56 days) to below 2000 Coulomb. A narrow range of values are identified for the mix design parameters, which provide flexibility for small deviations in the mixes to meet specific needs.

6.2 Fiber-Reinforced Polymer Bars

Two types of commercially available GFRP reinforcing bars (3/8"GFRP$_S$, and 3/8" & 1/2"GFRP$_R$) and one type of CFRP bars were studied in the project. A total of 105 bars were prepared, 32 of the bars were pre-conditioned with low temperature thermal cycling at eight

cycles per day. Specimens were exposed to 250 freeze-thaw cycles corresponding to 750 hours of exposure. Following 250 thermal cycles, the bars were visually examined for the development of cracks and then static and dynamic tension tests were performed to determine the ultimate tensile capacities of the FRP bars. Preliminary fatigue tests were performed to establish a definitive program for future study to determine the relationship of load range to the number of cycles to failure, and the effect of micro-cracking endured during freeze-thaw cycling.

The effect of the rate of loading on the tensile strength properties of glass fiber polymer reinforcements was investigated in order to establish a basis for cyclic fatigue loading procedures. The following conclusions have been made based on the analysis of the test results:

- The loading rate sensitivity of the strength of glass fiber reinforcing bars was quite apparent.

- There were noticeable increases in strength and marked changes in fracture appearance with increased loading rate.

- Freeze-thaw conditioning did have some deleterious effect on the ultimate strength of glass fiber polymer reinforcing bars.

- Stroke controlled tests produced more complete failure modes and repeatable load-displacement curves than load controlled tests.

- A basis for fatigue testing up to 2 Hz has been established.

- A complete experimental system and testing procedures are established for durability testing of FRP materials under environmental and mechanical loadings.

In order for FRP reinforcing bars to be successfully implemented in roadway construction projects, it is essential to develop a firm understanding of the durability properties of FRP bars and effects of exposure to severe and frequently changing environments. Preliminary results in this report show that freeze-thaw exposure may have some effects on the fatigue properties of

FRP bars. The degree of deterioration of the FRP bars depends on the temperature ranges and number of freezing-thawing cycles applied. Under the temperature conditions applied in this study, the decrease of the tensile strength of the FRP bars was no more than 10%. Although the temperature conditions in the tests were more severe than the actual temperature fluctuations in Colorado, the degradation of the tensile strength should be considered properly in structural design.

6.3   Pullout and Precast Panel Tests

Pullout test results show that 13-mm (0.5-in.) C-BAR reinforcing rods provided higher bond strength than #4 (13-mm diameter) black steel reinforcing bars. The average bond strength of the C-BAR with an embedment of $5d_b$ was 3.15 ksi. The average bond strength of the reinforcing steel with an embedment of $6d_b$ was 2.9 ksi. Pullout test results show that 10-mm (0.39-in.) Leadline prestressing tendons provided higher bond strength than 3/8-in. steel prestressing strand. The average bond strength of the Leadline with an embedment of $10d_b$ was 1.58 ksi. The average bond strength of the steel strand with an embedment of $20d_b$ was 0.99 ksi.

In this study, the panels prestressed with CFRP cannot be directly compared to those prestressed with steel due to the abnormalities in the construction of the CFRP prestressed panels. In the construction, the placement of the CFRP tendons in the panels nearly wiped out all eccentricity specified in design. Also, the panel depth was reduced by 0.1 in. Finally, the concrete strength on the day of testing was 3,600 psi instead of the specified 56 day strength of 4,500 psi. Lastly, cracks developed near the CFRP prestressing tendons before testing. The prestressing force was released while the concrete strength was at 2,500 psi which was very low compared to the specified release strength of 4,300 psi. This could be very likely the cause of the cracks. With all of the above problems, the load carrying capacity of the panel was 9.9 kips which is much lower than expected.

The steel prestressed panels did not have any of the construction problems discussed for the CFRP prestressed panels. In fact, the concrete strength for the steel prestressed panels was 40 5,800 psi on the panel testing day. This was significantly larger than the 4,500 psi strength

specified in design. The actual load carrying capacity reached was 21.6 kips in the panel test.

A careful analysis has indicated that the CFRP panel should have performed satisfactorily if it was constructed properly. The testing of a panel that was removed from the actual bridge added a great deal of confidence in the performance of a properly constructed CFRP prestressed panel. Unlike the first CFRP panel discussed above, the load carrying capacity obtained in testing was larger than the theoretical load carrying capacity.

Each panel that was tested showed a load carrying capacity greater than the equivalent construction load of 5 kips. The CFRP prestressed panel, steel prestressed panel, and the CDOT CFRP prestressed panel (removed from the I-225/Parker Road bridge) had load carrying capacities of 9.9 kips, 21.6 kips, and 42.3 kips, respectively.

In the case of the two composite slabs, the load carrying capacities attained in the tests were either greater than or close to the theoretical load carrying capacities. The load carrying capacities for the steel prestressed composite slab and the CFRP prestressed composite slab were 96.6 kips and 81.4 kips, respectively. As a result of the problems mentioned above, the failure of the CFRP prestressed slab was governed by tendon slip, and, therefore, had a lower resistance than the steel prestressed slab. The wheel load of the HS25-44 AASHTO design truck with alternate military loading and an impact factor is 26 kips.

The results of the moment analysis using the strain data show that the steel reinforced slab better distributed the loading in the transverse direction than the FRP reinforced slab. This would imply that the GFRP bars in the panels might not be as effective as the steel bars for distributing the load. Hence, the recommendation in the ACI 440H draft report for FRP temperature reinforcement may not be adequate for distribution reinforcement.

6.4   Fatigue Testing of Bridge Deck

From the load resistance standpoint, CFRP bars seem to be a viable alternative to steel tendons for precast panel construction. The portion of the bridge deck that had CFRP prestressed

panels demonstrated the same performance as that with steel prestressed panels. In the example considered in this report, the limit-state design method developed in this project resulted in a reinforcement quantity that is comparable to the empirical method of AASHTO. The former is, however, a more rational approach based on a rigorous analytical procedure.

The test results show that the segments of the deck that had the topping slabs designed with the empirical method and the limit-state method exhibited the same performance as that designed with the conventional method, even though the latter required 70% more reinforcement in the topping slab. Furthermore, with the use of the empirical method, the segment (segment A) of the deck that had precast panels performed better than the full-depth cast-in-place segment (segment D) due to the enhanced strength and crack resistance introduced by the prestressed panels.

The use of the AASHTO empirical method for the design of the topping slab of a precast panel deck does not seem to jeopardize the deck performance under fatigue load cycles. The empirical method can lead to a significant reduction of the top reinforcement in such a deck. It will not only save construction costs, but will also prolong the life span of a bridge deck that has steel reinforcement by reducing corrosion problems. Therefore, it is recommended that the empirical method be allowed for the design of the topping slab for precast panel decks.

The limit-state design method proposed in this project will result in a reinforcement quantity that is comparable to the empirical method of AASHTO. The former is, however, a more rational approach based on a rigorous analytical procedure. With more calibration and evaluation, this method can be adopted in the design practice.

7. References

1. AASHTO (1996), *Standard Specifications for Highway Bridges.* 16th Ed., American Association of State Highway and Transportation Officials, Washington, D.C.

2. AASHTO (1998), *Standard Specifications for Highway Bridges - LRFD.* 2nd Ed., American Association of State Highway and Transportation Officials, Washington, D.C.

3. Cusson, R. and Xi, Y. (2003), "The Behavior of Fiber-Reinforced Polymer Reinforcement in Low Temperature Environmental Climates." *Report No. CDOT-DTD-R-2003-04*, Colorado Department of Transportation, Denver, CO.

4. Shing, P.B. and Abu-Hejleh, N. (1999), "Cracking in Bridge Decks: Causes and Mitigation." *Report No. CDOT-DTD-R-99-8*, Colorado Department of Transportation, Denver, CO.

5. Shing, P.B., Borlin, K.A., and Marzahn, G. (2003), "Evaluation of a Bridge Deck with CFRP Prestressed Panels under Fatigue Load Cycles." *Report No. CDOT-DTD-R-2003-11*, Colorado Department of Transportation, Denver, CO.

6. Xi, Y., Shing, B., and Xie, Z. (2001), "Development of Optimal Concrete Mix Designs for Bridge Decks." *Report No. CDOT-DTD-R-2001-11*, Colorado Department of Transportation, Denver, CO.

7. Zylstra, R., Shing, P.B., and Xi, Y. (2001), "Evaluation of FRP Prestressed Panels/Slabs for I-225/Parker Road Project." *Report No. CDOT-DTD-R-2001-14*, Colorado Department of Transportation, Denver, CO.